Discovery of new diaryl ether inhibitors against Mycobacterium tuberculosis targeting the minor portal of InhA

Mélina Chebaiki, Evelyne Delfourne, Rasoul Tamhaev, Saïda Danoun, Frédéric Rodriguez, Pascal Hoffmann, Emeline Grosjean, Fernanda Goncalves, Joëlle Azéma-Despeyroux, Adrián Pál, et al.

Discovery of new diaryl ether inhibitors against *Mycobacterium tuberculosis* targeting the minor portal of InhA

Mélina Chebaiki,[a,b] Evelyne Delfourne,[a] Rasoul Tamhaev,[a,b] Saïda Danoun,[a] Frédéric Rodriguez,[a] Pascal Hoffmann,[a] Emeline Grosjean,[a] Fernanda Goncalves,[a] Joëlle Azéma-Despeyroux,[a] Adrián Pál,[c] Jana Korduláková,[c] Nadège Preuilh,[b] Sébastien Britton,[b] Patricia Constant,[b] Hedia Marrakchi,[b] Laurent Maveyraud,[b,*] Lionel Mourey,[b,**] Christian Lherbet[a,***]

[a] Synthèse et Physico-Chimie de Molécules d'Intérêt Biologique (LSPCMIB), UMR 5068, CNRS, Université Toulouse III – Paul Sabatier (UPS), Toulouse, France.

[b] Institut de Pharmacologie et de Biologie Structurale (IPBS), Université de Toulouse, CNRS, Université Toulouse III – Paul Sabatier (UPS), Toulouse, France.

[c] Department of Biochemistry, Faculty of Natural Sciences, Comenius University in Bratislava, Mlynská dolina, Ilkovičova 6, 84215 Bratislava, Slovakia.

[*] Corresponding author.

[**] Corresponding author.

[***] Corresponding author.

E-mail addresses: laurent.maveyraud@ipbs.fr (L. Maveyraud), lionel.mourey@ipbs.fr (L. Mourey). christian.lherbet@univ-tlse3.fr (C. Lherbet).

Keywords: Tuberculosis, InhA, minor portal, diaryl ether, coumarin, mechanism, cytotoxicity.

ABSTRACT

Tuberculosis (TB) caused by *Mycobacterium tuberculosis* (Mtb) affects 10 million people each year and the emergence of resistant TB augurs for a growing incidence. In the last 60 years, only three new drugs were approved for TB treatment, for which resistances are already emerging. Therefore, there is a crucial need for new chemotherapeutic agents capable of eradicating TB. Enzymes belonging to the type II fatty acid synthase system (FAS-II) are involved in the biosynthesis of mycolic acids, cell envelope components essential for mycobacterial survival. Among them, InhA is the primary target of isoniazid (INH), one of the most effective compounds to treat TB. INH acts as a prodrug requiring activation by the catalase-peroxidase KatG, whose mutations are the major cause for INH resistance. Herein a new series of direct InhA inhibitors were designed based on a molecular hybridization approach. The new compounds exhibit potent inhibitory activities of InhA and, for some of them, good antitubercular activities. Moreover, they display a low toxicity on human cells. A study of the mechanism of action of the most effective molecules shows that they inhibit the biosynthesis of mycolic acids. The X-ray structures of two InhA/NAD^+/inhibitor complexes have been obtained showing a binding mode of a part of the molecule in the minor portal, rarely seen in the InhA structures reported so far.

1. Introduction

Tuberculosis (TB) has existed for millennia and is still considered a scourge. It is the second leading causes of death due to a single pathogen worldwide, after the COVID-19 pandemic. Based on the Global Tuberculosis Report 2022, 1.6 million people died from TB and an estimated 10 million people fell ill with TB in 2021 [1]. Although TB is considered curable, the coronavirus crisis has caused distortions in its diagnosis and treatment in many countries, which has made patients all the more vulnerable. In addition, the emergence of multidrug-resistant TB (MDR-TB) and extensively-drug resistant TB (XDR-TB) strains remains a challenge. In this context, various actions, including the discovery of new drugs, have to be taken to move towards the eradication of TB. The unique composition of the mycobacterial cell envelope has led researchers to focus on the proteins involved in the biosynthesis of its major components, mycolic acids. The biosynthesis of these essential and very specific α-alkylated β-hydroxylated fatty acids involved two fatty acid synthase (FAS) systems called FAS-I and FAS-II. In FAS-II, at least four independent enzymatic activities participate to the elongation of the FAS-I products: β-hydroxyacyl-ACP (acyl carrier protein) synthase (MabA), enoyl-ACP reductase (InhA), β-hydroxyacyl-ACP dehydratase complex (HadABC), and β-ketoacyl-ACP synthase (KasA/KasB). Isoniazid (INH) is one of the oldest drugs for tuberculosis treatment. This small molecule acts as a prodrug, requiring the prior activation by the catalase peroxidase enzyme KatG. Upon activation, the isonicotinoyl radical forms an adduct with the cofactor NAD, which inhibits InhA, leading to the arrest of mycolic acid biosynthesis and the mycobacterium death [2]. With the emergence of INH resistance, mainly due to mutations in KatG, new direct inhibitors of InhA have emerged. These include triclosan (TCL) [3] and TCL derivatives [4-7], GEQ and analogues [8, 9], triazoles [10], thiazoles [11], pyridomycin [12, 13], and 4-hydroxy-2-pyridones [14]. Furthermore, GlaxoSmithKline's thiadiazole GSK693 [15] and the diazaborine AN12855 [16] were two promising leads with low toxicity, good oral bioavailability, *in vivo* efficacy similar to INH, and above all, activity against *katG*-deficient Mtb. However, none of the above compounds has been approved for clinical use. Thus, there is still a need to develop new direct inhibitors which overcome INH resistance.

In this respect, being a key target for antitubercular drug discovery, InhA has been the subject of numerous structural studies by X-ray crystallography. In 1995, its structure was the very first from the Mtb proteome to be deposited in the protein data bank (PDB) [17] and there are currently 105 deposited structures compared to 80 in the last comprehensive review published in 2018 [18]. Crystal structures corresponding to the *apo*-form and to complexes with its NAD cofactor, a substrate analogue and various inhibitors, including the INH-NAD adduct and the above listed direct inhibitors, have been resolved at resolution ranging from 3.4 to 1.4 Å. This allowed defining the most important structural elements with regard to the mechanisms of action and inhibition. InhA is a tetrameric

enzyme with dihedral (D2) symmetry where the four subunits are related by three 2-fold axes. The tertiary fold consists of a central seven-stranded parallel β-sheet sandwiched on each side by three helices. One of the two helical faces is overhung by two additional helices, H5 and H6, which form the so-called "substrate-binding loop" (SBL). Opposite the SBL and in the extension of the β-sheet and the other helical face, there are two loops (A and B). The SBL and loops A and B line the InhA active site, which forms a deeply buried crevice. At the bottom of the crevice and spanning the C-termini of the β-strands is the cofactor binding site. Above the cofactor binding site is found the substrate binding site, one end of which is wide open to the solvent via the major portal while at the apex of the opposite side is the much smaller minor portal [19]. The catalytic triad, composed of residues Phe149-Tyr158-Lys165, is located under the entrance of the minor portal. The conformation of the SBL loop, more specifically the position of helix H6, and the orientation of the Phe149 and Tyr158 side chains are important structural descriptors related to the different states of the enzyme, i.e. *apo*, *holo*, in complex with inhibitors. All inhibitors, except the three inhibitors INH-NAD adduct, pyridomycin, and AN12855 compound, bind to the enzyme in the presence of the cofactor. A very few of the InhA inhibitors for which an X-ray structure has been deposited within the PDB reach the entrance to the minor portal: 8PP (5-octyl-2-phenoxyphenol, ligand ID 8PS in PDB 2B37) [20], PT155 (5-(4-amino-2-methylphenoxy)-2-hexyl-1-methylpyridin-4(1*H*)-one, ligand ID 1S5 in PDB 4OXK) [21], and AP-124 ((S)-1-(benzo[*d*]imidazol-1-yl)-3-(2,3-dihydro-1*H*-inden-5-yl)oxy)propan-2-ol, ligand ID JVZ in PDB 6R9W) [22]. The alkyl diphenyl ether 5-octyl-2-phenoxyphenol is one example of the many triclosan-based InhA inhibitors, which represent one quarter of all InhA structures in the PDB [5, 9, 20, 21, 23-27].

Here, we report the design and synthesis, based on a molecular hybridization approach, of a series of new diaryl ethers bearing various, mainly coumarinic, heterocycles **(Fig. 1)**. This strategy, which consists in combining two molecules or molecular fragments to obtain a more affine compound for the target, was proven successful to discover new antitumor or anti-Mtb agents [28, 29]. We show that these new diaryl ethers exhibit excellent inhibition of both InhA activity and mycobacterial growth. The mechanism of action of these compounds were also investigated through monitoring the effect on mycolic acid biosynthesis in Mtb and cytotoxic activity. Finally, the binding mode of these molecules was elucidated through the determination of high-resolution X-ray structures of complexes, which revealed that these compounds are able to occupy the minor portal, to an extent never observed before.

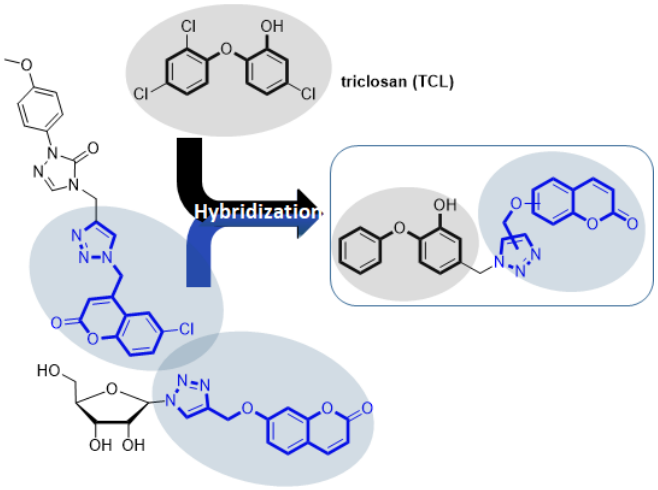

Figure 1. *Design of the new diaryl ether inhibitors by a molecular hybridization approach based on TCL and coumarins.*

2. Results and discussion

2.1. Design of the hybrid inhibitors

First structure-activity studies on TCL have shown that this diaryl ether molecule may bind at two sites of the InhA substrate-binding pocket [9]. One TCL molecule (TCL1) was found to bind through π-stacking interactions between the hydroxyl-substituted ring, hereafter called " A ring", and the nicotinamide ring of the cofactor plus hydrogen bonding between the hydroxyl moiety of the A ring and the 2'-hydroxyl group of NAD^+ and hydroxyl group of Tyr158. The dichlorophenyl ring (or "B ring") is orthogonally oriented to the A ring. It is worth mentioning that the TCL1-binding site occupies the part of the substrate-binding site, as observed in the structure of the complex with a C16 fatty acyl substrate analogue, which is directly accessible through the major portal [19]. The second TCL molecule (TCL2) binds to the remaining part of the substrate-binding site in a rather hydrophobic region close to the minor portal. This spatial configuration of TCL1 and TCL2, which underlines the size of the InhA binding site, has been exploited to further develop TCL-based inhibitors of the enzyme [5, 7, 20, 21, 23-27, 30-33]. In the resolved structures of InhA complexes with TCL derivatives, the diaryl ether moiety systematically binds in the same position as TCL1 whereas the various chemical substituents, at position 5 of the A ring, reach the space occupied by the TCL2 A ring **(Fig. 2)**. The hydroxyl group of the phenol moiety revealed as essential for activity by dictating the orientation of the molecules in the substrate-binding site (for a review, see [34]). In 2006, Sullivan *et al*. developed a series of alkyl diphenyl ethers bearing an alkyl chain up to 14 carbons on the A ring. The molecule showing the best inhibitory activity, both on InhA and on the growth of Mtb, bears a 8 carbon-long alkyl chain (IC_{50} = 5 nM, MIC(H37Rv) = 6.4 µM) [20]. Later, Freundlich *et al*. diversified the nature of

the substituents on the A ring with branched alkyl chains or alkyl chains containing (hetero)aromatic groups, but this did not lead to improved activities against InhA [23]. On the other hand, Stec *et al.* showed that the introduction of a triazole group among various heterocycles at position 5 exhibited favorable interactions with the protein, the best compound carrying a *n*-butyl chain on the position 4 of the triazole [7]. Lately, Spagnuolo *et al.* observed that large and bulky substituents at position 5 on the A ring induce steric hindrance in the substrate-binding site resulting in the loss of key interactions [27, 34]. Despite this, we and others thought that bulkier substituents at the 5-position could target the space occupied by TCL2. For instance, we recently reported the synthesis of macrocyclic *di*-triclosan analogues which displayed good inhibitory activity against InhA (IC_{50} = 4.7 µM) [32]. Chetty et *al.* also developed a series of flexible *di*-triclosan analogues revealing inhibition in the same range [35]. To go further, we decided to replace the diaryl ether corresponding to the TCL2 site with coumarin derivatives. Indeed, the coumarin skeleton is a privileged scaffold in life sciences and is present in numerous biologically relevant natural or synthetic products. Such molecules display various biological activities such as antibacterial [36], antifungal [37], anti-Alzheimer [38], antioxidant [39], and antitumor [40, 41]. Some of them have also been studied as potential InhA and FabI inhibitors **(Fig. 1)** [42-44]. We speculated that coumarin moieties could mimic the second molecule of TCL as in the PDB structure 1P45 (chain A, hereafter 1P45:A) and interact with the rather hydrophobic residues defining the TCL2 site. These coumarins could be grafted to the diaryl ether scaffold with an appropriate linker. The 1,2,3-triazole pharmacophore introduced by click-chemistry through copper(I) azide-alkyne cycloaddition (CuAAC) was chosen as a spacer, as illustrated in **Fig. 1**.

*2.2. In silico studies of compound **7a***

Preliminary molecular docking was performed to evaluate the ability of compound **7a (Fig. 3A)** to bind into the substrate-binding site of the enzyme. With the aim of exploring the possible interactions and conformation of the compounds, we used two X-rays structures. The first one corresponds to the 1P45:A coordinates, where the binding of two TCL molecules has been observed with an open major portal and a closed minor portal. The second X-ray structure corresponds to the complex of InhA with PT70 (2-(o-tolyloxy)-5-hexylphenol, compound TCU in PDB 2X22, chain A, hereafter 2X22:A) in which the major portal is closed and the minor portal is opened.[25] Two flexible docking protocols (MSE and OPT) were applied giving four results per ligand and two docking scores per result (see Experimental section 4.2.1. for pose selection, strength and conformity). With 1P45:A, U-shaped conformations of **7a** were obtained whatever the docking protocol used (**Fig. 3B**). Fluctuations were limited and the hydrogen bonding network between Tyr158, the cofactor, the ligand, and the π-π interactions involving the nicotinamide group with the phenol group of **7a** were similar to TCL1 (Supporting

Information **Fig. S1**) whereas the coumarin group occupies the same place as TCL2. In contrast, S-shaped-like conformations were observed using 2X22:A, with the coumarin reaching the minor portal **(Fig. 3C**). The diaryl ether moiety of **7a** showed the same interactions as TCL1 in 1P45:A and PT70/TCU in 2X22:A pattern (Supporting Information **Fig. S2**). Furthermore, by superimposing the strongest poses obtained after docking of **7a** in 2X22:A, fluctuations starting from the triazole were observed in the minor portal **(Fig. 3D)**. It has to be noted that the averaged fluctuations (positions and orientations) of coumarin were found similar using the two docking protocols. Interestingly, the docking scores regardless of protocol were better for compound **7a** in 2X22:A than in 1P45:A.

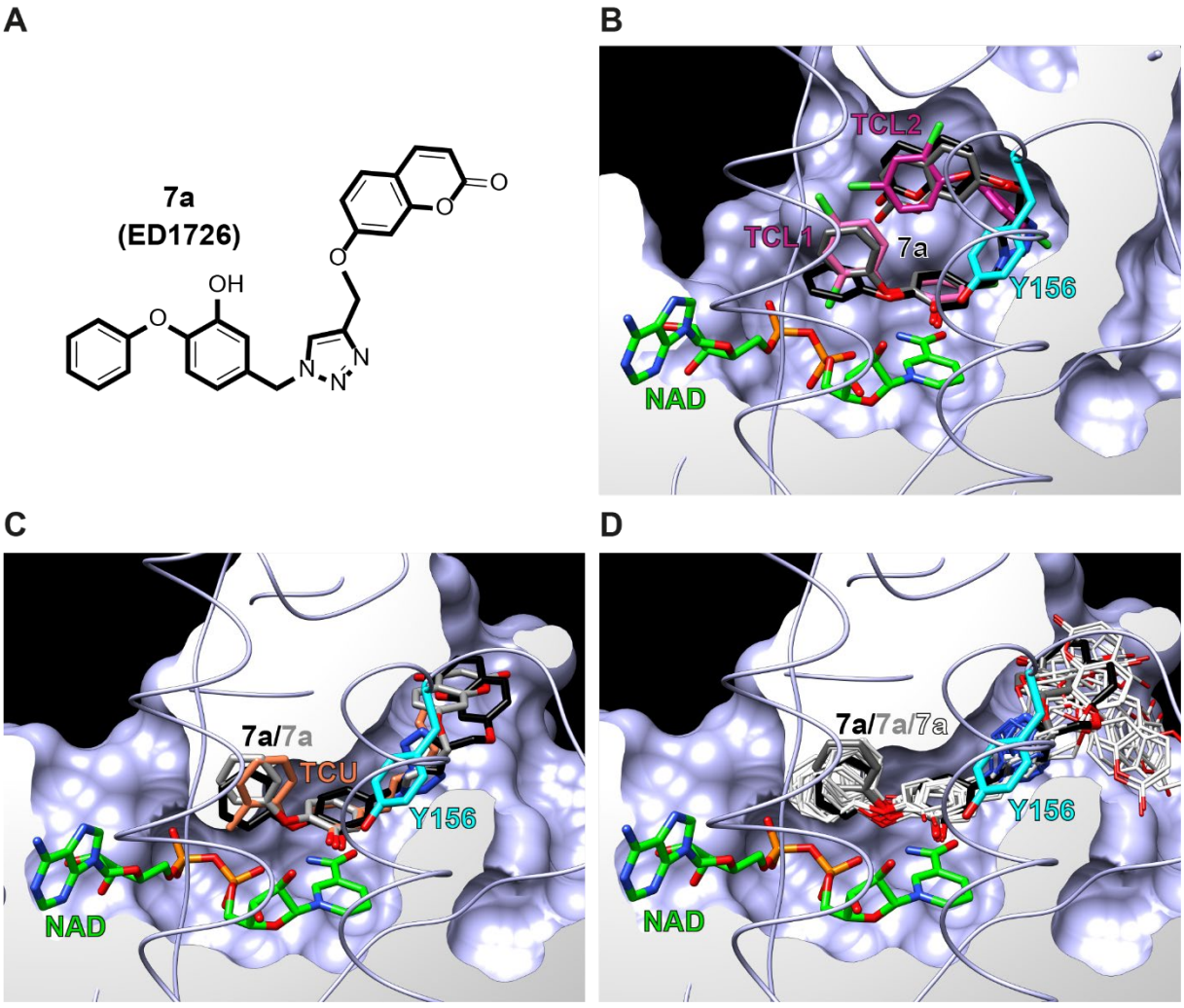

Figure 3. **A.** Compound **7a** used for docking. **B.** Best poses obtained using the MSE and OPT docking protocols of **7a** (black and dark gray sticks, respectively) in 1P45:A (lightblue ribbon and surface) relatively to Tyr158 (cyan). The two TCL molecules (pink) and NAD (green) of 1P45:A are also shown. **C**. Best poses obtained using the MSE and OPT docking protocols of **7a** (black and dark gray sticks, respectively) in 2X22:A (lightblue ribbon and surface) relatively to Tyr158 (cyan). The TCU (brightorange) and NAD (green) molecules of 2X22:A are also shown. **D**. Fluctuations of the ten best poses (MSE and OPT docking protocols, white) of **7a** in 2X22:A (lightblue ribbon and surface) relatively

to Tyr158 (cyan) and NAD (green). The two best poses displayed in panel C are also shown (black and gray sticks).

2.3. Synthesis of the designed inhibitors

Based on our knowledge of the InhA binding site and docking results on compound **7a**, several molecules have been conceived and are described in schemes 2 and 3. The azidomethyl derivatives **5a-c** were prepared in four steps from the corresponding aldehydes **1a-c,** themselves obtained according to procedures previously described **(Scheme 1)** [45, 46].

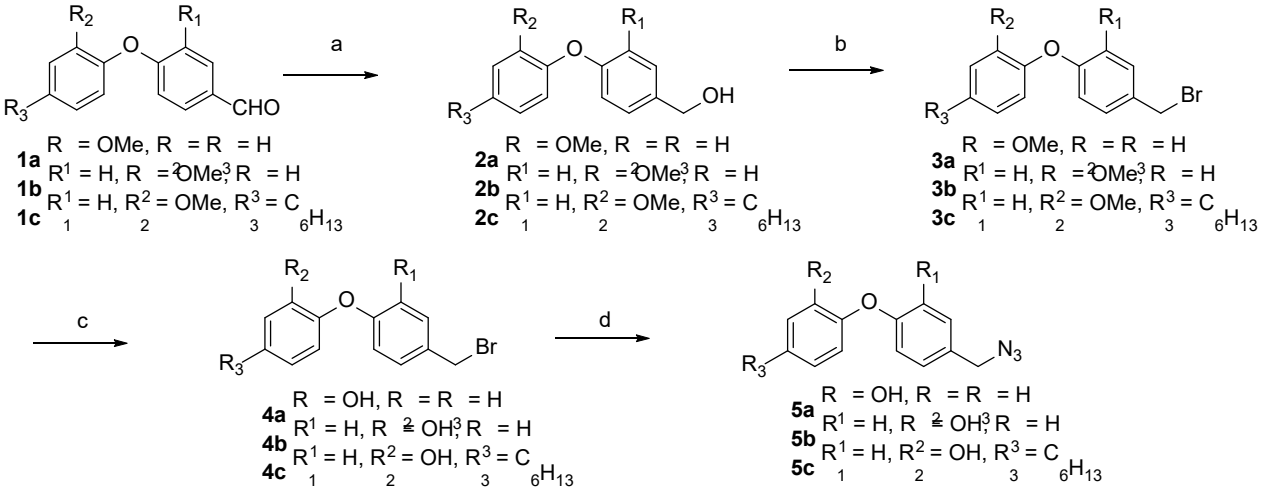

(a) $NaBH_4$, MeOH, RT, 3 h, **2a** quantitative, **2b** 94%, **2c** 74%. (b) NBS, PPh_3, CH_2Cl_2, RT, 3 h, **3a** 95%, **3b** 76%, **3c** 47%. (c) BBr_3, CH_2Cl_2, - 78 °C, 4 h, **4a** 94%, **4b**, 38%, **4c** 27%. (d) NaN_3, DMF, 45°C, 4 h, **5a** 86%, **5b** quantitative, **5c** quantitative.

Scheme 1. Synthesis of the azidomethyl derivatives.

Briefly, a sequence of reduction, bromation and demethylation by BBr_3 provided compounds **4a-c**. Deprotection was preferable at this stage, in terms of yield, rather than once the Huisgen's products **7a-n** were obtained. Even knowing this, an effective demethylation reaction is compound-dependent. The synthesis of compound **4a** was achieved in 94%, while for compounds **4b** and **4c,** moderate yields were obtained with 38 and 27%, respectively. These compounds were finally transformed into their corresponding azidomethyl derivatives by action of NaN_3 in DMF, synthons **5a-c** being so obtained in 77, 27 and 9% overall yield respectively. Described procedures were used to dispose of the propargyl derivatives **6a-c** (see Supporting Information) [47, 48]. Compound **6d** was synthesized in 38% yield, by action of propargyl bromide and potassium carbonate on 7-(diethylamino)-4-hydroxycoumarin [49] in DMF. Compounds **6e-i** were prepared involving the corresponding coumarinic acid derivatives and carbodiimidazole in dichloromethane whereas intermediates **6j-k** were synthesized through well-known protocols (see Supporting Information). The Huisgen's 1,3-dipolar azide-alkyne cycloaddition of

azidomethyl derivatives **5a-c** with the propargyl derivatives **6a-k** proceeded in yield ranging from 44 to 87% to give the triazoles **7a-n** as indicated in **Scheme 2**. The synthesis of 1,2,3-triazole derivatives **7a-n** has been achieved by Cu(I)catalyzed Huisgen-Sharpless-Meldal [3+2] azide-alkyne dipolar cycloaddition (CUAAC) [50, 51] of azidomethyl phenoxyphenols **5a**-**c** with propargyl coumarins **6a-i** and extended to propargyl benzoxadiazoles **6j-k (Scheme 2)**.

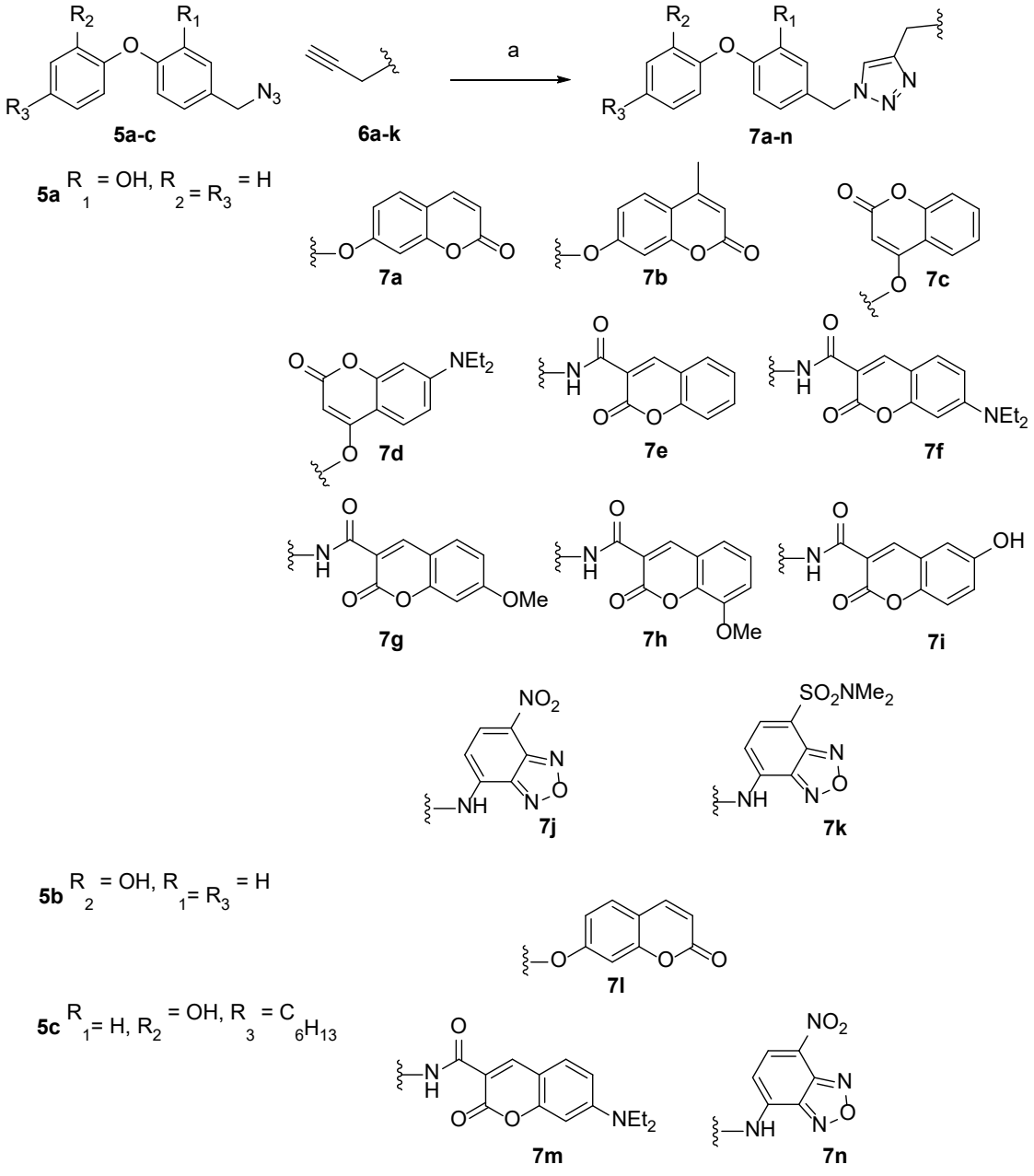

Scheme 2. Synthesis of the various diaryl ether derivatives **7a-n** by CuAAC click chemistry.

In order to compare their inhibitory activity to that of 1,4-triazoles, two 1,5-triazole regioisomers were prepared *via* the ruthenium-catalyzed azide alkyne cycloaddition (RuAAC) [52]. Azide **5a** was reacted

with alkynes **6a** or **6b** in the presence of $Cp^*RuCl(PPh_3)_2$ as catalyst to furnish 1,5- disubstituted 1,2,3-triazole derivatives **8a** and **8b** in low yields **(Scheme 3)**.

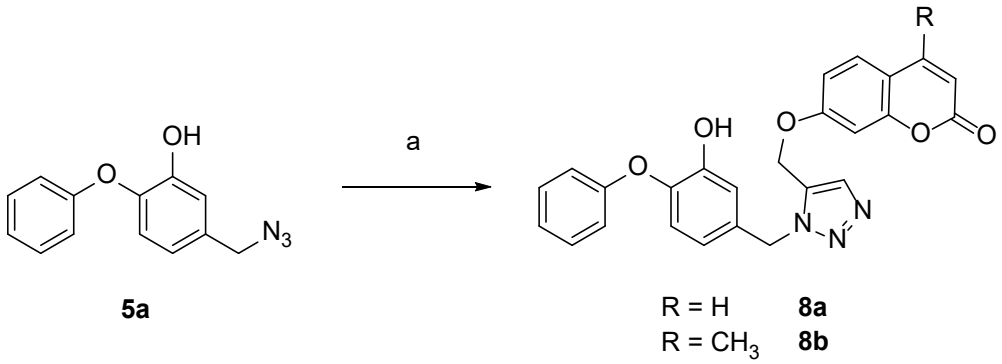

(a) **6a** or **6b**, $Cp^*RuCl(PPh_3)_2$, dioxane: **8a** (35%), **8b** (29%)

Scheme 3. Synthesis of 1,5-triazole derivatives **8a** and **8b** v*ia* a ruthenium-catalyzed azide-alkyne cycloaddition (RuAAC).

2.4. InhA inhibition

In order to choose appropriate fragments for the development of inhibitors targeting the minor portal of InhA, twenty-two compounds including some alkynyl precursors, azide **5a** and 1,4- and 1,5-triazole derivatives were screened for their inhibitory potency against InhA. The assays were performed in the presence of 2-*trans*-dodecenoyl-CoA and NADH. The molecules were firstly tested at 500 µM for the alkyne precursors and 50 µM for the "click" derivatives. For the most potent inhibitors, IC_{50} values were determined **(Table 1)**. The general trend shows that alkyne precursors exhibit low inhibitory activities compared to triazole products or even to the azide **5a**. These results clearly show that the protein does not recognize these alkynic precursors. Diaryl ether azide **5a** showed good inhibition with an IC_{50} of 0.843 µM. Compound **7d** bearing 7-diethylaminocoumarin substituted at the position 4 showed the best inhibitory activity with 0.053 µM, a 15-fold increase in comparison to **5a**. Replacement of the 7-diethylamino substituent by hydrogen (compound **7c**) resulted in a decrease of the activity. Comparison of compounds **7a** and **7l**, which only differ in the position of the hydroxyl group, showed the importance of this group which will dictate the positioning of the rest of the molecule by interacting with Tyr158. Coumarin-3-carboxamides **7e-7i** were less active but with very important differences in inhibition depending on the substituent and its position on the coumarin. 7-Diethylamino coumarin **7f** exhibited an IC_{50} of 3.5 µM while less bulky 7-methoxy-coumarin derivative **7g** was 10 fold more active with an IC_{50} of 0.345 µM. Replacing coumarins by nitrobenzoxadiazole (NBD) or 4-(*N*,*N*-dimethylaminosulfonyl)benzoxadiazole (DBD) as found in **7j** and **7k** did not result in better inhibition. Two other compounds, **7m** and **7n**, bearing a C_6-alkyl chain, were evaluated. These

compounds are analogues to one of the most potent inhibitors of InhA, 5-hexyl-2-phenoxyphenol showing nanomolar inhibition of InhA enzyme but poor MIC (69 µM) [20]. The C_6-alkyl chain plays a crucial role in interacting with the rather hydrophobic region close to the minor portal in the protein substrate-binding site. The presence of the C_6 chain and the position of the hydroxyl group guide the positioning of the NBD and coumarin heterocycles toward the major portal. The two molecules showed weak inhibitory activity against the InhA enzyme **(Table 1)**. Finally, 1,5-triazole regioisomers **8a** and **8b** showed slightly weaker inhibition by comparison with **7a** and **7b,** with IC_{50} of 0.630 µM and 0.510 µM, respectively. This represents a drop in inhibition of only 2.5 to 3.8 times. These results show that 1,5-triazole derivatives despite a very different conformational space compared with 1,4-triazoles have the ability to inhibit the InhA protein.

Table 1. Activities against InhA enzyme and Mtb H37Rv strain.

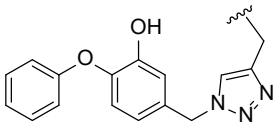

7a-7k

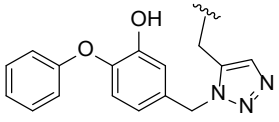

8a-8b

Compound	R	IC_{50} (µM or % at concentration Tested)	MIC H37Rv µg/mL (µM)
5a	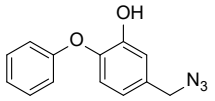	0.843 ± 0.094	NT
6a	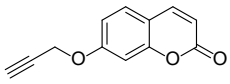	200 µM: 99% 100 µM: 30%	NT
6b	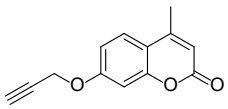	500 µM: 90% 200 µM: 37%	NT
6c	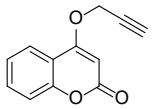	500 µM: NI	NT
6e	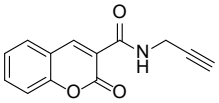	200 µM: NI	NT
6f	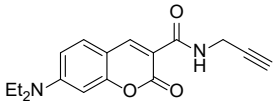	500 µM: 10%	NT
7a **ED1726**	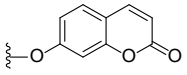	0.163 ± 0.017	2.2 (5)
7b	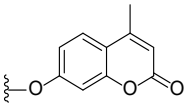	0.205 ± 0.012	0.6 (1.25)

	ED1727		
7c	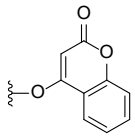	0.181 ± 0.016	2.2 (5)
	ED1728		
7d	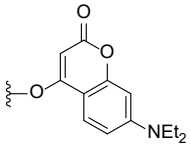	0.054 ± 0.015	0.7 (1.25)
	ED1834		
7e	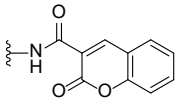	0.598 ± 0.061	4.7 (10)
	ED1751		
7f	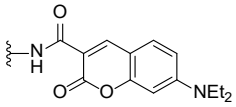	3.550 ± 1.030	>54 (>100)
	ED1765		
7g	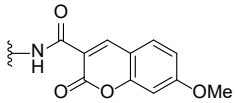	0.345 ± 0.029	>5 (>10)
	ED1806		
7h	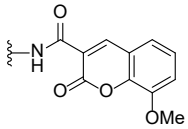	0.740 ± 0.150	5 (10)
	ED1769		
7i	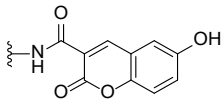	0.844 ± 0.095	>4.8 (>10)
	ED1786		
7j	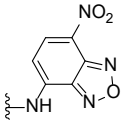	0.459 ± 0.040	4.6 (10)
	ED1755		
7k	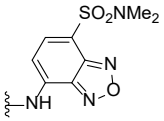	0.733 ± 0.065	>52 (>100)
	ED1758		
7l	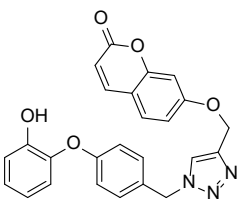	50 µM: 10%	2.2 (5)
	ED1750		

7m	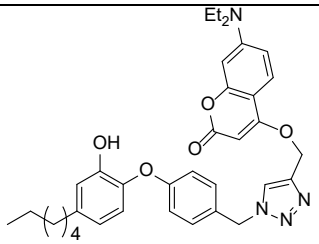 **EG1-090**	50 µM: 53.7% 10 µM: 31.5% 1 µM: 14.1%	>60 (>100)
7n	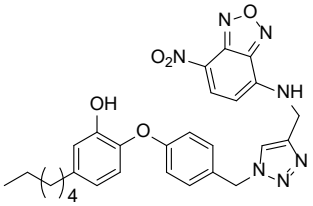 **EG1-093**	50 µM: 32.3% 10 µM: 11.4%	1.4 (2.5)
8a	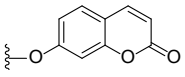 **MC3-121**	0.630 ± 0.050	NT
8b	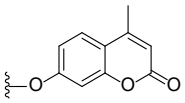 **MC3-122**	0.510 ± 0.060	NT
Ciprofloxacine		NA	0.8 (2.5)

NT: not tested, NI: no inhibition, NA: not applicable.

2.5. Antimycobacterial activity

Table 1 lists the inhibitory activity of the growth of Mtb H37Rv for each 1.4-triazole derivatives. Ciprofloxacine was used for comparison. MIC values obtained are very disparate, ranging from 1.25 µM to >100 µM. Two compounds, **7b** and **7d**, which display good inhibitory activity against InhA, were found to inhibit mycobacterial growth with MICs of 1.25 µM. Interestingly, these two active compounds are different by the positioning of the connection to the coumarin but also by the nature of the substituents that the coumarin carries. Compound **7a** bearing no substituent, by comparison with compound **7b,** shows a greater MIC (5 µM). 7-Des(diethylamino) compound **7c** compared to **7d** loses effectiveness. Coumarin amide **7e-7i** presented MICs values higher than 10.0 µM. Surprisingly, compounds **7l** and **7n**, which displayed poor inhibitory activity against InhA, could inhibit Mtb growth with MICs of 5.0 and 2.5 µM, respectively, while **7m** shows no activity. Therefore, we believe that these two compounds might have biological targets other than InhA.

2.6. Inhibition of mycolic acid biosynthesis in Mtb H37Rv

The effect of the three best anti-tubercular compounds, i.e. **7b**, **7d** and **7n**, on the biosynthetic pathway of mycolic acids was investigated by metabolic labeling of pathogenic bacteria Mtb H37Rv with ^{14}C acetate. Treatment of Mtb H37Rv with three concentrations of compounds **7b** and **7d** corresponding to 1x, 5x, and 25x their MIC leads to a decreased production of lipids containing mycolic acids, namely trehalose monomycolates (TMM) and trehalose dimycolates (TDM) **(Fig. 4A)**, as well as all types (alpha, methoxy, keto) of mycolic acids and accumulation of standard fatty acids (FAME) **(Fig. 4B)**. These results are consistent with the potential of compounds **7b** and **7d** to inhibit the production of mycolic acids and their derivatives in mycobacterial cells. Of note, treatment with biaryl ether derivative **7n** displays a distinct inhibition profile and leads to the accumulation of trehalose monomycolates and decreased production of trehalose dimycolates while it has no effect on the production of mycolic acid **(Fig. 4B)**. This result correlates with the fact that compound **7n** is a poor InhA inhibitor. This imbalance of TMM/TDM ratio in favor of TMM was reported upon the inhibition of the TMM transporter, MmpL3, using either small-molecule inhibitors [53, 54], or in conditional mycobacterial *mmpL3* mutants [55].

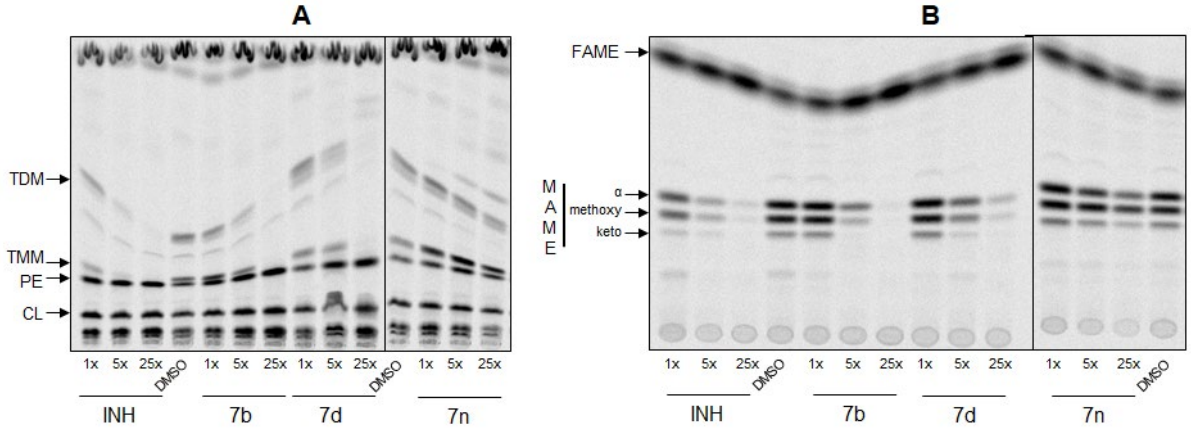

Figure 4. TLC analysis of lipids after metabolic labeling experiment of mycobacteria treated with compounds **7b**, **7d**, or **7n** for the analysis of lipid inhibition (A) and for the analysis of mycolic acid inhibition (B). **7b** (1.25 µM 1×, 6.25 µM 5×, 31.25 µM 25×), **7d** (1.25 µM 1×, 6.25 µM 5×, 31.25 µM 25×), **7n** (2.5 µM 1×, 12.5 µM 5×, 62.5 µM 25×). Abbreviations: FAME: Fatty Acid Methyl Esters, MAME: Mycolic Acid Methyl Esters; TDM: Trehalose DiMycolates; TMM: Trehalose MonoMycolates; PE: PhosphatidylEthanolamine; CL: CardioLipin.

2.7. Sensitivity of Mtb H37Ra strains overproducing KatG/InhA/HadABC

The mechanism of action of **7b**, **7d**, and **7n** was investigated by using H37Ra strains carrying pVV16-*katG*$_{smeg}$, pMV261-*inhA* and pVV16-*hadABC* constructions overexpressing catalase peroxidase KatG, InhA and HadABC dehydratases, respectively. H37Ra strains carrying empty vectors pMV261 and pVV2 were used as controls. The same sensitivity of Mtb H37Ra strains overproducing KatG and HadABC comparing to the control strains means that the important HadABC component of the FASII system is not the target of the compounds and, as expected, these compounds are not activated by the KatG protein **(Table 2)**. In contrast, the increased MIC of **7b** and **7d** in Mtb H37Ra overproducing InhA confirms InhA as the specific target.

Table 2. Sensitivity of Mtb H37Ra strains overproducing KatG/InhA/HadABC to **7b**, **7d** and **7n**.

Mtb strains	**MIC (µM)**		
	7b	**7d**	**7n**
H37Ra pMV261	1.25-6.25	6.25	2.5-12.5
H37Ra pVV2	1.25-6.25	6.25	2.5-12.5
H37Ra pVV16-*katG*$_{smeg}$ *(2)*	1.25-6.25	6.25	2.5-12.5
H37Ra pVV16-*katG*$_{smeg}$ *(4)*	1.25-6.25	6.25	2.5-12.5
H37Ra pMV261-*inhA (1)*	12.5	>25	2.5-12.5
H37Ra pMV261-*inhA (2)*	12.5	>25	2.5-12.5
H37Ra pVV16-*hadABC*	1.25-6.25	6.25	2.5-12.5

2.8. Cytotoxic activity on human cell lines

The cytotoxic activity of compounds **7b**, **7d** and **7n** was evaluated after 72 h of treatment on a panel of various human cell lines including the colon carcinoma HCT116 cell line, the HepG2 hepatocarcinoma cell line (which can recapitulate the metabolization of some compounds into toxic secondary metabolites), the CACO2 colorectal carcinoma cell line (used as a model of the intestinal epithelial barrier) and WI38hTERT, which are normal lung fibroblasts immortalized by telomerase expression. These assays revealed that compound **7b** has only weak cytotoxic effects, especially against lung fibroblasts (>100 µM, Selectivity Index>80). Compound **7n** exhibited moderate cytotoxicity against the panel tested, while **7d** was clearly cytotoxic. These results show that the nature of coumarin plays an important role in the cytotoxicity of these compounds.

Table 3. Cytotoxicity of compounds **7b**, **7d** and **7n**.

Compound	MIC (µM)	IC_{50} (µM)/Selectivity Index[a]			
	H37Rv	HCT116	CACO2	HepG2	WI38hTERT
7b	1.25	23.9/19.1	25/20	31/24.8	>100/>80
7d	1.25	0.53/0.4	1.1/0.9	1.6/1.3	0.6/0.5
7n	2.5	8.70/3.5	26.1/10.5	26.9/10.8	52.9/21.2

[a] The selectivity index corresponds for each compound to the ratio between the IC_{50} on the tested human cell line and the MIC on Mtb H37v. MIC and IC_{50} established from three independent experiments.

2.9. X-ray structures

In parallel to the characterization of the compounds for their ability to inhibit the enzymatic activity of InhA and mycobacterial growth, a massive crystallization campaign of the corresponding complexes was launched in order to rationalize the results obtained. The structures of the complexes with compounds **7b** and **7e** could be resolved, after incubation in the presence of NAD^+, at resolutions of 1.60 and 1.96 Å, respectively **(Table S1)**. From the more than one hundred X-ray structures of InhA available in the PDB, it appears that the protein and its complexes can be crystallized in different conditions leading to different space groups with one, two, four, six or eight molecules in the corresponding asymmetric units. The InhA/NAD^+/**7b** complex (PDB code 8OTN) crystallized in the presence of PEG 4000 in space group ($P2_12_12_1$ with cell parameters a=70.16 Å, b=91.18 Å, c=164.22 Å and 4 molecules in the asymmetric unit. The InhA/NAD^+/**7e** (PDB code 8OTM) complex also crystallized in the presence of PEG 4000 and with 4 molecules in the asymmetric, but in a different space group ($P2_1$ with a=90.59 Å, b=92.78 Å, c=90.75 Å, β=119.20°). In both X-ray structures, all four molecules in the asymmetric unit are almost complete, only missing one or two residues at their N and C termini. When superimposing based on Cα atoms, the different molecules in the asymmetric unit for each structure or the two structures between them, the calculated RMSD values do not exceed 0.3 Å, showing that the tertiary structures of InhA in the two complexes are almost identical. Furthermore, in both structures, the SBL loop is in closed conformation and the orientation of the Phe149 and Tyr158 side chains are in the so-called *out* and *in* conformation, respectively **(Fig. 5A)**. The NAD^+ is positioned in the cofactor binding site where it adopts the canonical conformation observed in all InhA structures through several hydrogen bonds and hydrophobic interactions. As expected, compounds **7b** and **7e** bind similarly above the cofactor with the diaryl ether moiety in the same position as that found in the structures of InhA-TCL complexes, e.g. TCL1 in 1P45:A (see **Fig. 2**), the hydroxyl-substituted ring being stacked with the nicotinamide ring of the cofactor and the phenyl ring pointing towards the major portal. The orientation of the triazole with respect to the diaryl ether and its conformation is also the

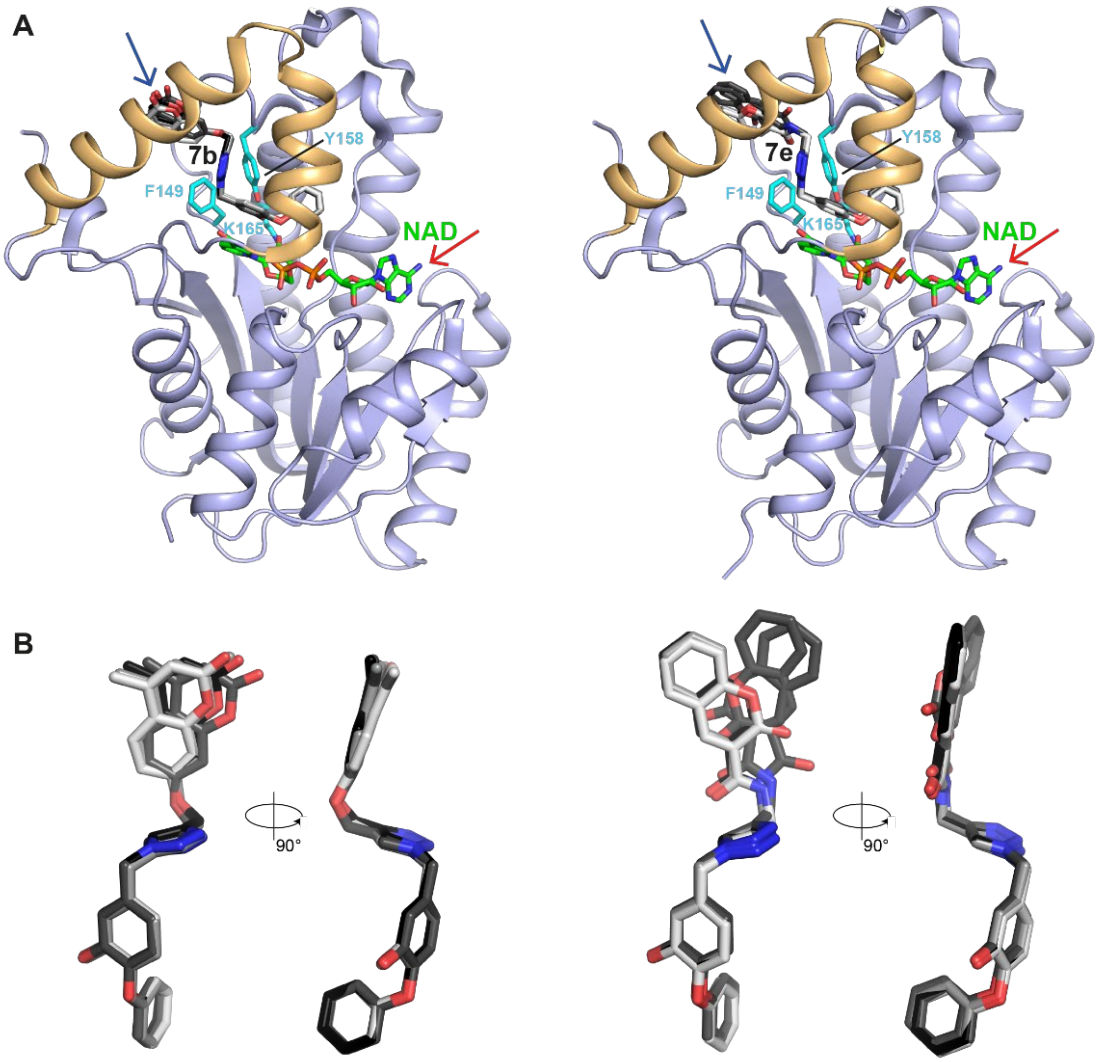

Figure 5. X-ray structures of InhA/NAD$^+$/**7b** (left) and InhA/NAD$^+$/**7e** (right). **A.** Overall structure. Cartoon representation of InhA/NAD$^+$/**7b** (8OTN, chain D) and InhA/NAD$^+$/**7e**, (8OTM, chain B) with the NAD$^+$ (green), the ligand (shades of grey) and the side chains of the catalytic triad Phe149-Tyr158-Lys165 (cyan) shown as sticks. The SBL loop is shown in orange. Red and blue arrows in panel A indicate the active site entrance and minor portal, respectively. **B.** Two perpendicular zoom-in views showing the fluctuations of the coumarin part of the ligands in the four molecules found in the respective asymmetric unit (shown in A. and B. as different shades of grey).

same for **7b** and **7e**, as well as in other structures with triazole-containing diphenyl ethers [24, 27], but fluctuations are observed for the coumarin part of the ligands in the four molecules found in the respective asymmetric units **(Fig. 5B)**. As TCL1 in 1P45:A, hydrogen bonds are found between the hydroxyl moiety of the diphenyl ether with the hydroxyl group of Tyr158 and the 2'-hydroxyl group of NAD$^+$ **(Fig. 6)**. In addition, binding of both compounds occurs through non-bonded contacts invariably involving the cofactor and residues Gly96, Phe97, Met98, Phe149, Met155, Pro156, Ala157, Tyr158, Met161, Ala198, Met199, Ile202, Val203, Gln214, Leu217, Leu218. In some instances, the very tip of the Arg225 side chain from the same protomer and the C-terminal residues, Leu268 and Leu269, of a

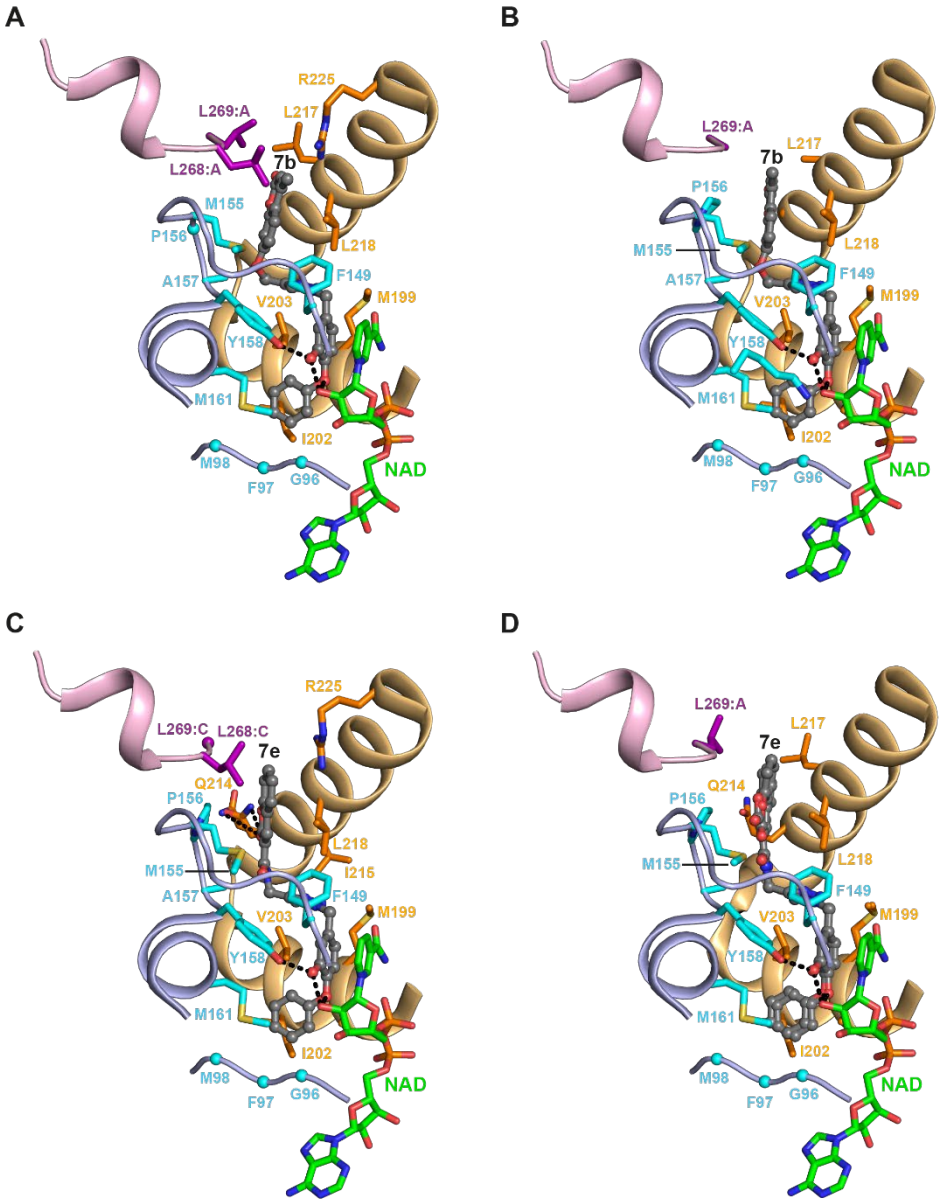

Figure 6. Detailed description of **7b** and **7e** binding to InhA/NAD$^+$. The two most extreme conformations of the coumarin part observed for **7b** (resp. **7e**) are displayed in panels **A.** and **B.** (resp. **C.** and **D.**). The protein is shown as cartoon using the same color scheme as in Fig. 5. The cofactor is in green. Protein residues involved in defining the inhibitor-binding pocket are shown as cyan sticks (side chain atoms involved) or spheres (only main chain atoms are involved) and labeled. Hydrogen bonds are displayed as black dotted lines.

contacting protomer from the tetramer may complete the inhibitor-binding pocket **(Fig. 6)**. Altogether, this allows to completely embed the diphenyl ether, the triazole and the coumarin phenyl moiety of **7b** (resp. the coumarin lactone of **7e**) whereas the coumarin lactone of **7b** (resp. the coumarin phenyl moiety of **7e**) is pointing out of the open crevice above the minor portal **(Fig. 6)**. The overall conformations observed for **7b** and **7e** are reminiscent of the S-shaped conformation obtained after molecular docking of the **7a** compound. It is noteworthy that the fluctuations observed for the coumarin part in the X-ray structures do not impact the positions and conformations of the InhA

residues involved in non-bonded contacts, except for the side chains of residues Gln214 and Leu 217 and those of Leu268 and Leu269 of the contacting protomer, which allows fine adjustment. In the case of **7b**, these fluctuations are of low amplitude **(Fig. 6A, B)**. The flexibility of the coumarin part is more important in the case of the complex with **7e** where in chain A, it is stabilized through hydrogen bonding between the carbonyl oxygen atom of the lactone and the NED2 atom in one of the two conformations of Gln214 (**Fig. 6C**), whereas in chain C, the C6-N1-C7-C8 amide dihedral bond adopts two alternate conformations resulting in the flipping of the C7-O3 bond without strongly affecting the orientation of the coumarin (**Fig. 6D)**.

The X-ray structures obtained for **7b** and **7e** show how a diaryl ether-based hybrid inhibitor can explore the exit of the InhA minor portal in a way never seen before for triclosan derivatives. It has been previously shown that two such derivatives (i.e. compound 8PS and 1S5 in PDB 2B37 and 4OXN, respectively) can only reach the entrance of this unexplored part of the enzyme (Supporting Information **Fig. S4**). Future works will deal with the design of more potent diaryl ether-triazole hybrid inhibitors bearing original substituents which can provide anchors.

3. Conclusions

A hybridization strategy, based on a diaryl ether structural scaffold and coumarinic fragments, allows the design of new inhibitors able to explore underexploited regions in InhA. The docking results carried out on one of the targeted molecules **7a**, show two binding modes in the active site of InhA, which depend on the chosen structure of InhA i.e 1P45:A or 1X22:A with major and minor portals more or less closed. Encouraged by these results, biaryl ether derivatives bearing various coumarins, or benzoxadiazoles moieties were synthesized in a few steps in high yields. Among them, two molecules **7b** and **7d** exhibited very good anti-Mtb efficiency and were able to block mycolic acid biosynthesis in Mtb H37Rv. Studies of their mechanism of action confirmed that InhA is their target. Two structures of the complexes InhA/NAD^+ with compounds **7b** and **7e** could be resolved. They reveal the binding of the coumarin moiety with a wide fluctuation, into the minor portal to a level never seen before. These structures represent a good opportunity for researchers interested in InhA to explore this finally accessible binding site. Further works, including structural optimization as well as pharmacological and toxicological studies, are now needed to evaluate the relevance of these molecules as anti-TB drugs.

4. Experimental section

4.1. Chemistry experimental

4.1.1. Material and methods

All commercially available chemical solvents and reagents were used without further purification. ^{1}H and ^{13}C were recorded on a Bruker Avance 600 (600 MHz and 151 MHz respectively); Bruker Avance 500 (500 MHz and 125 MHz, respectively) or a Bruker Avance 300 spectrometer (300 MHz and 75 MHz, respectively). The chemical shift values are reported in ppm using the solvent residual peak as internal reference: $CDCl_3$ δ = 7.26 ppm/77.0 ppm, DMSO-d_6 δ = 2.50 ppm/39.52 ppm and the coupling constants (*J*) are in Hz, while multiplicities are abbreviated by s (singlet); bs (broad singlet); d (doublet); dd (doublet of doublets); ddd (doublet of doublets of doublets); t (triplet); td (triplet of doublets); tt (triplet of triplets); m (multiplet). * = the multiplicity of the signal is more complex as it is part of an AA'XX' system. High-resolution mass spectra (HRMS) were recorded on a GCT Premier spectrometer upon electron spray ionization (ESI) or chemical ionization (DCI, CH_4). Follow up of the reaction outcome by thin-layer chromatography (TLC) was performed on precoated Merck silica gel 60F-254 plates using an appropriate solvent system and the different spots were detected under UV lamp (λ 254 nm or 360 nm). Flash chromatography were performed using a Puriflash®300 with silica columns.

All the compounds were dissolved in acetonitrile before analysis by a Waters Acquity UHPLC-DAD-MS (Ultra Performance Liquid Chromatography with Diode Array Detector). The separations were achieved on a Waters Acquity BEH Phenyl (100 mm x 2.1 mm, particle size 1.7 µm) column. The mobile phase consisted of water with 0.1% formic acid (solvent A) and acetonitrile with 0.1% formic acid (solvent B) at a flow rate of 0.4 $mL.min^{-1}$. The temperature of the column oven was set at 30 °C. The chromatographic analysis consisted in a linear gradient program from 60% A/40% B to 0% A/100% B between 1 and 12 min. After each run, the percentage of solvents ramped to their initial composition in 2 min and then the column was re-equilibrated for 2 min. The UV detection were performed at Lambda max of each compound and UV-Vis spectra were recorded within a range of 200-800 nm. The presence of possible impurities was evaluated at different wavelengths. The data acquisition and processing were done with the Empower 2 software. All tested compounds were more than 95% pure, as established by HPLC.

The synthesis of 3-methoxy-4-phenoxybenzaldehyde **(1a)** [45], 4-(2-methoxyphenoxy)benzaldehyde (**1b**) [46], 7-(prop-2-yn-1-yloxy)-2H-chromen-2-one **(6a)** [48], 4-methyl-7-(prop-2-yn-1-yloxy)-2H-chromen-2-one (**6b)** [47], 4-(prop-2-yn-1-yloxy)-2H-chromen-2-one (**6c)** [47], 7-Nitro-N-(prop-2-yn-1-yl)benzo[c][1,2,5]oxadiazol-4-amine **(6j)** [56], and *N*,*N*-dimethyl-7-(prop-2-yn-1-ylamino)benzo[c][1,2,5]oxadiazole-4-sulfonamide **(6k)** [57] have been previously described and the observed chemical shifts in NMR are in accordance with the published data. The synthesis and the spectroscopic data of aldehyde derivative **1c** and propynyl coumarins **6e-6h** are described in the Supporting Information.

4.1.1. Synthesis of the derivatives

(4-Benzyl-3-methoxyphenyl)methanol (2a). To a solution of aldehyde **1a** (860 mg, 3.77 mmol) in methanol (43 mL) was added portion wise sodium borohydride (728 mg, 18.85 mmol). The mixture was stirred at room temperature for 3 h and water (50 mL) was added. After concentration under reduced pressure, the mixture was extracted with dichloromethane (3 x 50 mL). The combined organic layers were dried over $MgSO_4$ and concentrated under reduced pressure. No further purification was necessary. The expected compound **2a** was isolated quantitatively as a white solid, R_f = 0.34 (petroleum ether/ethyl acetate: 80/20). ^{1}H NMR ($CDCl_3$, 300 MHz) δ 7.33-7.27 (m, 2H); 7.07-7.02 (m, 2H); 6.97-6.92 (m, 3H); 6.89 (dd, *J* = 8.2, 1.9 Hz, 1H); 4.69 (s, 2H); 3.85 (s, 3H). ^{13}C NMR ($CDCl_3$, 75 MHz) δ 157.8; 151.3; 144.2; 137.6; 129.4 (2C); 122.4; 120.8; 119.3; 117.0 (2C); 111.5; 64.8; 55.8. HRMS (DCI-CH_4, $[M]^+$) calculated for $C_{14}H_{14}O_3$ 230.0943, found 230.0937.

(4-(2-Methoxyphenoxy)phenyl)methanol (2b). Same procedure as for compound **2a**, involving aldehyde **1b** (340 mg, 1.49 mmol) in methanol (17 mL), sodium borohydride (290 mg, 7.45 mmol). The crude product was purified by flash chromatography (petroleum ether/ethyl acetate: 80/20) to give compound **2b** as a colourless oil (320 mg, 94%); R_f = 0.08 (petroleum ether/ethyl acetate: 80/20). ^{1}H NMR ($CDCl_3$, 300 MHz) δ 7.29 (d*, *J* = 8.7 Hz, 2H); 7.14 (ddd, *J* = 8.3, 7.1 Hz, 2.0 Hz, 1H); 7.03-6.89 (m, 5H); 4.65 (s, 2H); 3.84 (s, 3H). ^{13}C NMR ($CDCl_3$, 75 MHz) δ 157.5; 151.4; 144.9; 134.9; 128.5 (2C); 129.9; 121.1; 121.1; 117.1 (2C); 112.8; 64.9; 55.9. HRMS (DCI-CH_4, $[M]^+$) calculated for $C_{14}H_{14}O_3$ 230.0943, found 230.0954.

(4-(4-Hexyl-2-methoxyphenoxy)phenyl)methanol (2c). Same procedure as for compound **2a**, involving aldehyde **1c** (645 mg, 2.09 mmol) in methanol (30 mL) sodium borohydride (397 mg, 10.5 mmol). The crude product was purified by flash chromatography (gradient dichloromethane/ethyl acetate: 100/0 to 90/10) to give compound **2c** as a white solid (608 mg, 90%), R_f = 0.60 (dichloromethane/ethyl acetate: 90/10). ^{1}H NMR ($CDCl_3$, 300 MHz) δ 7.26 (d*, *J* = 8.8 Hz, 2H); 6.93-6.87 (m, 3H); 6.82 (d, *J* = 1.9 Hz, 1H); 6.74 (dd, *J* = 8.0 Hz, 2.0 Hz, 1H); 4.60 (s, 2H); 3.81 (s, 3H); 2.61 (t, *J* = 8.0 Hz, 2H); 1.96 (bs, 1H); 1.63 (quint, *J* = 7.7 Hz, 2H); 1.42-1.30 (m, 6H); 0.91 (t, *J* = 7.0 Hz, 3H). ^{13}C NMR ($CDCl_3$, 75 MHz) δ 157.8; 151.1; 142.4; 140.0; 134.6; 128.4 (2C); 121.0; 120.7; 116.8 (2C); 113.0; 64.8; 55.9; 35.8; 31.7; 31.5; 29.0; 22.6; 14.0. HRMS (DCI-CH_4, $[M+H]^+$) calculated for $C_{20}H_{27}O_3$ 315.1960, found: 315.1960.

4-(Bromomethyl)-2-methoxy-1-phenoxybenzene (3a). To a solution of alcohol **2a** (140 mg, 0.609 mmol, 1 eq) and triphenylphosphine (416 mg, 1.58 mmol) in dry dichloromethane (7 mL) was added portion wise *N*-bromosuccinimide (282 mg, 1.58 mmol). The mixture was stirred at room temperature for 3 h. After concentration under reduced pressure, the crude product was purified by flash chromatography (petroleum ether/ethyl acetate: 70/30) affording compound **3a** as a white solid (169 mg, 95%); R_f = 0.62 (petroleum ether/ethyl acetate: 70/30). ^{1}H NMR ($CDCl_3$, 300 MHz) δ 7.34-7.28 (m, 2H); 7.07 (tt, *J* = 7.4 Hz, 1.4 Hz, 1H); 7.03 (d, *J* = 2.0 Hz, 1H); 6.98-6.92 (m, 3H); 6.87 (d, *J* = 8.1 Hz, 1H); 4.51 (s, 2H); 3.87 (s, 3H). ^{13}C NMR ($CDCl_3$, 75 MHz) δ 157.3; 151.2; 145.6; 134.0; 129.6 (2C); 122.9; 121.7; 120.3; 117.7 (2C); 113.4; 56.0; 33.6. HRMS (DCI-CH_4, $[M+H]^+$) calculated for $C_{14}H_{14}BrO_2$ 293.0177, found 293.0167.

1-(4-(Bromomethyl)phenoxy)-2-methoxybenzene (3b). Same procedure as for compound **3a** involving alcohol **2b** (290 mg, 1.26 mmol), triphenylphosphine (860 mg, 3.27 mmol, 2.6 eq), dry dichloromethane (15 mL), *N*-bromosuccinimide (583 mg, 3.27 mmol). The crude product was purified by flash chromatography (petroleum ether/ethyl acetate: 90/10) to give compound **3b** as a white solid (280 mg, 76%); R_f = 0.55 (petroleum ether/ethyl acetate: 70/30). ^{1}H NMR ($CDCl_3$, 300 MHz) δ 7.31 (d*, *J* = 8.7 Hz, 2H); 7.16 (ddd, *J* = 8.4, 7.2, 2.0 Hz, 1H); 7.01 (dd, *J* = 8.1, 1.8 Hz, 2H); 6.94 (ddd, *J* = 8.1 Hz, 7.2 Hz, 1.8 Hz, 1H); 6.88 (d*, *J* = 8.7 Hz, 2H); 4.50 (s, 2H); 3.82 (s, 3H). ^{13}C NMR ($CDCl_3$, 75 MHz) δ 158.2; 151.6; 144.3; 131.5; 130.4 (2C); 125.3; 121.6; 121.2; 116.9 (2C); 112.8; 55.9; 33.6. HRMS (DCI-CH_4, $[M+H]^+$) calculated for $C_{14}H_{14}BrO_2$ 293.0177, found 293.0177.

1-(4-(Bromomethyl)phenoxy)-4-hexyl-2-methoxybenzene (3c). To a solution of alcohol **2c** (489 mg, 1.56 mmol) in dry dichloromethane (10 mL) at 4 °C under argon, was added phosphorous tribromide (549 g, 2.03 mmol, 1.3 eq). After 3 h, methanol (5 mL) was added. The solvent was removed *in vacuo* and the crude product was dissolved in dichloromethane. The organic mixture was washed with water, dried over $MgSO_4$, filtered and concentrated *in vacuo*. Purification by flash chromatography (gradient petroleum ether/dichloromethane: 90/10 to 75/25) gave **3c** as a yellow oil (0.282 g, 47%), R_f = 0.35 (petroleum ether/dichloromethane: 90/10). ^{1}H NMR ($CDCl_3$, 300 MHz) δ 7.30 (d*, *J* = 8.8 Hz 2H); 6.92 (d, *J* = 8.0 Hz, 1H); 6.87 (d*, *J* = 8.8 Hz, 2H) ; 6.82 (d, *J* = 1.9 Hz, 1H); 6.75 (dd, *J* = 8.0 Hz, 1.9 Hz, 1H); 4.50 (s, 2H); 3.81 (s, 3H); 2.62 (t, *J* = 7.9 Hz, 2H); 1.64 (quint, *J* = 7.7 Hz, 2H); 1.42-1.27 (m, 6H); 0.90 (t, *J* = 6.8 Hz, 3H); ^{13}C NMR ($CDCl_3$, 75 MHz) δ 158.5; 151.2; 141.7; 140.5; 131.1; 130.3 (2C); 121.5; 120.7; 116.5 (2C); 112.9; 55.9; 35.8; 33.6; 31.6; 31.4; 28.9; 22.5; 14.0; HRMS (DCI-CH_4, $[M]^+$) calculated for $C_{20}H_{25}BrO_2$ 376.1038, found 376.1042.

5-(Bromomethyl)-2-phenoxyphenol (4a). To a solution of bromide **3a** (70 mg, 0.24 mmol) in dry dichloromethane (30 mL), boron tribromide (1 M solution in dichloromethane, 3 mL, 3.0 mmol) was added dropwise under argon atmosphere. The mixture was stirred at 4 °C for 4 h. Sodium bicarbonate saturated solution (40 mL) was added. The organic layer was separated and the aqueous layer was extracted with dichloromethane (2 x 40 mL). The combined organic layers were dried over $MgSO_4$ and concentrated *in vacuo*. The crude product was purified by flash chromatography (petroleum ether/ethyl acetate: 90/10) affording compound **4a** as a clear yellow oil (63 mg, 94%); R_f = 0.57 (dichloromethane). ^{1}H NMR ($CDCl_3$, 300 MHz) δ 7.40-7.33 (m, 2H); 7.18-7.13 (m, *J* = 7.4 Hz, 1.4 Hz, 1H); 7.10 (d, *J* = 2.1 Hz, 1H); 7.06-7.02 (m, 2H); 6.87 (dd, *J* = 8.3 Hz, 2.1 Hz, 1H); 6.80 (d, *J* = 8.3 Hz, 1H); 4.46 (s, 2H). ^{13}C NMR ($CDCl_3$, 75 MHz) δ 156.2; 147.2; 143.9; 134.1; 129.9 (2C); 124.0; 121.3; 118.4 (2C); 118.3; 116.8; 33.3. HRMS (DCI-CH_4, $[M]^+$) calculated for $C_{13}H_{11}BrO_2$ 277.9942, found 277.9937.

2-(4-(Bromomethyl)phenoxy)phenol (4b). Same procedure as for compound **4a** involving bromide **3b** (140 mg, 0.48 mmol), dry dichloromethane (60 mL), boron tribromide (1M solution in dichloromethane, 6 mL, 6.0 mmol). The mixture was stirred at 4 °C for 4 h. Sodium bicarbonate saturated solution (50 mL) was added. The organic layer was separated and the aqueous layer was extracted with dichloromethane (2 x 80 mL). The combined organic layers were dried over $MgSO_4$ and concentrated *in vacuo*. The crude product was purified by flash chromatography (petroleum ether/ethyl acetate: 90/10) affording compound **4b** as a white solid (51 mg, 38%); R_f = 0.49 (petroleum ether/ethyl acetate: 70/30). ^{1}H NMR ($CDCl_3$, 300 MHz) δ 7.36 (d*, *J* = 8.7 Hz, 2H); 7.11-7.04 (m, 2H; 6.98 (d*, *J* = 8.7 Hz, 2H); 6.93-6.83 (m, 2H); 5.57 (bs, 1H); 4.50 (s, 2H). ^{13}C NMR ($CDCl_3$, 75 MHz) δ 156.9; 147.5; 142.9; 132.9; 130.7 (2C); 125.2; 120.7; 119.4; 117.9 (2C); 116.4; 33.0. HRMS (DCI-CH_4, $[M+H]^+$) calculated for $C_{13}H_{12}BrO_2$ 279.0021, found 279.0021.

2-(4-(Bromomethyl)phenoxy)-5-hexylphenol (4c). To a solution of bromide **6c** (103 mg, 0.27 mmol) in dichloromethane (5 mL) at 80 °C, was added boron tribromide (1M) (1.08 mL, 4 eq). After 5 h, methanol (5 mL) was added. The solvent was removed *in vacuo* and the crude product was dissolved in dichloromethane (20 mL). The organic mixture was washed with water (20 mL), dried over $MgSO_4$, filtered and concentrated *in vacuo*. Purification of the crude product by flash chromatography (petroleum ether/dichloromethane: 70/30 to 50/50) gave compound **4c** as a white solid (27 mg, 27%), R_f = 0.33 (petroleum ether/dichloromethane: 60/40). ^{1}H NMR ($CDCl_3$, 300 MHz) δ 7.34 (d*, *J* = 8.8 Hz, 2H); 6.96 (d*, *J* = 8.8 Hz, 2H); 6.88 (d, *J* = 2.0 Hz, 1H); 6.82 (d, *J* = 8.2 Hz, 1H); 6.67 (dd, *J* = 8.2 Hz, 2.1 Hz, 1H); 5.37 (bs, 1H); 4.49 (s, 2H); 2.56 (t, *J* = 7.9 Hz, 2H); 1.59 (quint, *J* = 7.5 Hz, 2H); 1.39-1.26 (m, 6H); 0.90 (t, *J* = 6.7 Hz, 3H); ^{13}C NMR ($CDCl_3$, 75 MHz) δ 157.4; 147.3; 140.6; 140.4; 132.6; 130.7 (2C); 120.6;

119.4; 117.5 (2C); 116.2; 35.5; 33.1; 31.7; 31.3; 28.9; 22.6; 14.1. HRMS (DCI-CH_4, $[M]^+$) calculated for $C_{19}H_{23}BrO_2$ 362.0881, found 362.0883.

5-(Azidomethyl)-2-phenoxyphenol (5a). To a solution of bromide **4a** (170 mg, 0.61 mmol) in dry *N*,*N*-dimethylformamide (2 mL), was added sodium azide (97 mg, 1.48 mmol). The mixture was stirred at 45 °C for 4 h. Ethyl acetate (30 mL) and water (20 mL) were added, the organic layer was washed with water (2 x 20 mL). The combined organic layers were dried over $MgSO_4$ and concentrated under reduced pressure. The crude product was purified by flash chromatography (petroleum ether/ethyl acetate: 80/20) affording compound **5a** as a colourless oil (125 mg, 86%); R_f = 0.60 (petroleum ether/ethyl acetate: 70/30). ^{1}H NMR ($CDCl_3$, 300 MHz) δ 7.40-7.33 (m, 2H); 7.17-7.12 (tt, *J* = 7.4 Hz, 1.5 Hz, 1H); 7.06-7.02 (m, 3H); 6.86 (d, *J* = 8.3 Hz, 1H); 6.79 (dd, *J* = 8.3 Hz, 2.3 Hz, 1H); 5.64 (s, 1H); 4.28 (s, 2H). ^{13}C NMR ($CDCl_3$, 75 MHz) δ 156.3; 147.4; 143.5; 131.7; 129.8 (2C); 123.7; 120.3; 118.6; 118.1 (2C); 116.0; 54.2. HRMS (DCI-CH_4, $[M]^+$) calculated for $C_{13}H_{11}N_3O_2$ 241.0851, found 241.0845.

2-(4-(Azidomethyl)phenoxy)phenol (5b). Same procedure as for compound **5a** involving bromide **4b** (50 mg, 0.18 mmol), dry *N*,*N*-dimethylformamide (5 mL), sodium azide (13 mg, 0.2 mmol, 1.1 eq). The crude product was purified by flash chromatography (petroleum ether/ethyl acetate: 80/20) affording compound **5b** as a colourless oil, R_f = 0.46 (petroleum ether/ethyl acetate: 70/30). ^{1}H NMR ($CDCl_3$, 300 MHz) δ 7.28 (d*, *J* = 8.7 Hz, 2H); 7.15-7.00 (m, 4H); 6.93-6.83 (m, 2H); 4.31 (s, 2H). ^{13}C NMR ($CDCl_3$, 75 MHz) δ 156.9; 147.5; 143.1; 130.4; 129.9 (2C); 125.1; 120.7; 119.2; 118.0 (2C); 116.4; 54.1. HRMS (DCI-CH_4, $[M]^+$) calculated for $C_{13}H_{11}N_3O_2$ 241.0851, found 241.0869.

2-(4-(Azidomethyl)phenoxy)-5-hexylphenol (5c). To a solution of **5c** (27 mg, 0.07 mmol) in *N*,*N*-dimethylformamide (2 mL), was added sodium azide (190 mg, 0. 29 mmol). The reaction mixture was heated at 45 °C and stirred for 20 h. Diethyl ether was added to the mixture and the organic mixture was washed with water, dried over $MgSO_4$, filtered and concentrated affording compound **5c** as a colorless oil (24 mg, quant.), R_f = 0.35 (petroleum ether/dichloromethane: 60/40). ^{1}H NMR ($CDCl_3$, 300 MHz) δ 7.27 (d*, *J* = 8.6 Hz, 2H); 7.01 (d*, *J* = 8.7 Hz, 2H); 6.88 (d, *J* = 2.0 Hz, 1H); 6.82 (d, *J* = 8.2 Hz, 1H); 6.67 (dd, *J* = 8.2 Hz, 2.0 Hz, 1H); 5.42 (bs, 1H); 4.31 (s, 2H); 2.56 (t, *J* = 7.8 Hz, 2H); 1.66-1.56 (m, 2H); 1.37-1.26 (m, 6H); 0.89 (t, *J* = 6.9 Hz, 3H). ^{13}C NMR ($CDCl_3$, ppm) δ 157.3; 147.3; 140.6; 140.5; 130.2 129.9 (2C); 120.6; 119.2; 117.7 (2C); 116.2; 54.2; 35.5; 31.7; 31.3; 28.9; 22.6; 14.1. HRMS (DCI-CH_4, $[M\text{-}N_2\text{-}H]^+$) calculated for $C_{19}H_{22}NO_2$ 296.1651, found: 296.1649.

7-(Diethylamino)-4-(prop-2-yn-1-yloxy)-2H-chromen-2-one (6d). To a solution of 7-(diethylamino)-4-hydroxycoumarin (0.100 g, 0.429 mmol) in *N*,*N*-dimethylformamide, were added propargyl bromide (76 mg, 0.058 mL, 0.515 mmol) and potassium carbonate (119 mg, 0.858 mmol) at room temperature. The reaction mixture was stirred at 100 °C for overnight and then concentrated *in vacuo*. The crude material was dissolved in ethyl acetate and washed with water and brine. The organic layers were dried over $MgSO_4$, filtered and concentrated in vacuo. The crude product was purified by flash chromatography (gradient dichloromethane/methanol: 100/0 to 95/5) affording compound **6d** as a brown powder upon standing (0.038 g, 33%). ^{1}H NMR ($CDCl_3$, 300 MHz) δ 7.56 (d, *J* = 9.0 Hz, 1H); 6.55 (dd, *J* = 9.0 Hz, 2.5 Hz, 1H); 6.45 (d, *J* = 2.5 Hz, 1H); 5.52 (s, 1H); 4.79 (d, *J* = 2.4 Hz, 2H); 3.39 (q, *J* = 7.1 Hz, 4H); 2.63 (t, *J* = 2.4 Hz, 1H); 1.19 (t, *J* = 7.1 Hz, 6H); ^{13}C NMR ($CDCl_3$, 75 MHz) δ 165.3; 163.9; 155.8; 151.1; 123.9; 108.3; 103.4; 97.1; 86.4; 77.2; 76.3; 56.4; 44.7 (2C); 12.4 (2C). HRMS (DCI-CH_4, $[M]^+$) calculated for $C_{16}H_{17}NO_3$ 271.1208, found 271.1211.

General procedure for the azide-alkyne cycloaddition. A solution of azide (1.2 eq), alkyne (1 eq), $CuSO_4.5H_2O$ (0.1 eq) and sodium ascorbate (0.4 eq) in a mixture of methanol/water was stirred at room temperature overnight. Water (100 mL) and dichloromethane (50 mL) were added. The combined organic layers were washed with water (50 mL) and brine (50 mL) and dried over $MgSO_4$. After concentration in vacuo, the crude product was purified by flash chromatography affording the expected product.

7-((1-(3-Hydroxy-4-phenoxybenzyl)-1H-1,2,3-triazol-4-yl)methoxy)-2H-chromen-2-one (7a). General procedure for the azide-alkyne cycloaddition involving azide **5a** (50 mg, 0.208 mmol), alkyne **6a** (35 mg, 0.174 mmol), $CuSO_4.5H_2O$ (4.35 mg, 0.0174 mmol) and sodium ascorbate (14 mg, 0.0696 mmol) in a mixture methanol (2 mL), water (7 mL) and dichloromethane (20 mL). The crude product was purified by flash chromatography (petroleum ether/ethyl acetate: 90/10) affording compound **7a** as a white solid (27.5 mg, 74%), R_f = 0.12 (dichloromethane/methanol: 98/2). ^{1}H NMR (DMSO-d_6, 600 MHz) δ 9.69 (s, 1H); 8.34 (s, 1H); 7.99 (d, *J* = 9.5 Hz, 1H); 7.64 (d, *J* = 8.6 Hz, 1H); 7.31-7.28 (m, 2H); 7.17 (d, *J* = 2.5 Hz, 1H); 7.03-7.00 (m, 2H); 6.95 (d, *J* = 8.1 Hz, 1H); 6.91 (d, *J* = 2.1 Hz, 1H); 6.84-6.82 (m, 2H); 6.78 (dd, *J* = 8.2, 2.1 Hz, 1H); 6.30 (d, *J* = 9.5 Hz, 1H); 5.55 (s, 2H); 5.27 (s, 2H). ^{13}C NMR (DMSO-d_6, 151 MHz) δ 161.1; 160.2; 157.7; 155.3; 149.4; 144.3; 142.5; 142.2; 133.0; 129.6 (2C); 129.5; 125.0; 122.1; 121.9; 119.2; 116.7; 116.2 (2C); 112.9; 112.7; 112.6; 101.6; 61.7; 52.4. HRMS (ESI, $[M+H]^+$) calculated for $C_{25}H_{20}N_3O_5$ 442.1403, found 442.1405. Purity (HPLC): 96.3% at 320 nm (t_R = 3.012 min).

7-((1-(3-Hydroxy-4-phenoxybenzyl)-1H-1,2,3-triazol-4-yl)methoxy)-4-methyl-2H-chromen-2-one (7b). General procedure for the azide-alkyne cycloaddition involving azide **5a** (100 mg, 0.416 mmol), alkyne **6b** (75 mg, 0.348 mmol), $CuSO_4.5H_2O$ (8.7 mg, 0.035 mmol) and sodium ascorbate (28 mg, 0.14 mmol) in a mixture methanol (4 mL), water (9 mL) and dichloromethane (20 mL). Purification by flash chromatography (dicholoromethane/methanol: 99/1) gave product **7b** as a white solid (120 mg, 74%); R_f = 0.06 (petroleum ether/ethyl acetate: 80/20). ^{1}H NMR (DMSO-d_6, 500 MHz) δ 9.70 (s, 1H); 8.34 (s, 1H); 7.70 (d, *J* = 8.7 Hz, 1H); 7.32-7.27 (m, 2H); 7.16 (d, *J* = 2.5 Hz, 1H); 7.05 (dd, *J* = 8.8 Hz, 2.5 Hz, 1H); 7.01 (tt, *J* = 7.4 Hz, 1.1 Hz, 1H); 4.94 (d, *J* = 8.1 Hz, 1H); 6.90 (d, *J* = 2.1 Hz, 1H); 6.84-6.82 (m, 2H); 6.78 (dd, *J* = 8.2, 2.1 Hz, 1H); 6.23 (d, *J* = 1.3 Hz, 1H); 5.55 (s, 2H); 5.27 (s, 2H); 2.40 (d, *J* = 1.3 Hz, 2H). ^{13}C NMR (DMSO-d_6, 126 MHz) δ 161.0; 160.1; 157.7; 154.6; 153.4; 149.4; 142.5; 142.2; 133.0; 129.6 (2C); 126.5; 125.0; 122.1; 121.9; 119.2; 116.7; 116.2 (2C); 113.4; 112.6; 111.3; 101.6; 61.6; 52.4; 18.1. HRMS (ESI, $[M+H]^+$) calculated for $C_{26}H_{22}N_3O_5$ 456.1559, found 456.1554. Purity (HPLC): > 99.9% at 320 nm (t_R = 3.259 min).

4-((1-(3-Hydroxy-4-phenoxybenzyl)-1H-1,2,3-triazol-4-yl)methoxy)-2H-chromen-2-one (7c). General procedure for the azide-alkyne cycloaddition involving azide **5a** (56 mg, 0.233 mmol); alkyne **6c** (39 mg, 0.195 mmol), $CuSO_4.5H_2O$ (4.9 mg, 0.0195 mmol) and sodium ascorbate (16 mg, 0.078 mmol) in a mixture methanol (2.5 mL), water (7.5 mL) and dichloromethane (20 mL). Purification by flash chromatography (dichloromethane/methanol: 99/1) gave compound **7c** as a white solid (62 mg, 72%); R_f = 0.13 (dichloromethane/methanol: 98/2). ^{1}H NMR ($CDCl_3$, 500 MHz) δ 9.70 (s, 1H); 8.45 (s, 1H); 7.75 (d, *J* = 8.0 Hz, 1H); 7.65 (t_{app}, *J* = 7.7 Hz, 1H); 7.41 (d, *J* = 8.2 Hz, 1H); 7.32 (t, *J* = 7.3 Hz, 1H); 7.32 (t_{app}, *J* = 8.0 Hz, 2H); 7.01 (t_{app}, *J* = 7.1 Hz, 1H); 6.96 (d, *J* = 8.1 Hz, 1H); 6.92 (d, *J* = 1.6 Hz, 1H)); 6.83 (d, *J* = 8.1 Hz, 2H); 6.80 (dd, *J* = 7.9, 1.5 Hz, 1H); 6.17 (s, 1H); 5.58 (s, 2H); 5.43 (s, 2H). ^{13}C NMR ($CDCl_3$, 126 MHz) δ 164.3; 161.5; 157.7; 152.8; 149.4; 142.5; 141.2; 132.9; 132.8; 129.6 (2C); 125.4; 124.2 122.9; 122.1; 121.9; 119.2; 116.7; 116.5; 116.2 (2C); 115.1; 91.3; 62.8; 52.5. HRMS (ESI, $[M+H]^+$) calculated for $C_{25}H_{20}N_3O_5$ 442.1403, found 442.1400. Purity (HPLC): 95.3% at 280 nm (t_R = 3.330 min).

7-(Diethylamino)-4-((1-(3-hydroxy-4-phenoxybenzyl)-1H-1,2,3-triazol-4-yl)methoxy)-2H-chromen-2-one (7d). General procedure for the azide-alkyne cycloaddition involving azide **5a** (38 mg, 0.158 mmol), alkyne **6d** (36 mg, 0.133 mmol), $CuSO_4.5H_2O$ (4 mg, 0.00133 mmol) and sodium ascorbate (11 mg, 0.0052 mmol) in a mixture methanol (2 mL), water (5 mL) and dichloromethane (10 mL). Purification by flash chromatography (dichloromethane/methanol: 98/2) gave product **7d** as a pale-yellow solid (55 mg, 81%), R_f = 0.13 (dichloromethane/methanol: 98/2). ^{1}H NMR ($CDCl_3$, 300 MHz) δ 7.63 (s, 1H (H_{15})); 7.54 (d, *J* = 9.0 Hz, 1H); 7.40-7.33 (m, 2H); 7.16 (tt, *J* = 7.5 Hz, 1.1 Hz, 1H); 7.05-7.01

(m, 2H); 6.98 (d, *J* = 2.1 Hz, 1H); 6.85 (d, *J* = 8.2 Hz, 1H); 6.77 (dd, *J* = 8.2 Hz, 2.2 Hz, 1H); 6.55 (dd, *J* = 8.9, 2.4 Hz, 1H); 6.47 (d, *J* = 2.4 Hz, 1H); 5.81 (s, 1H); 5.54 (s, 1H); 5.50 (s, 2H); 5.28 (s, 2H); 3.39 (q, *J* = 7.1 Hz, 4H); 1.19 (t, *J* = 7.1 Hz, 6H). ^{13}C NMR ($CDCl_3$, 75 MHz) δ 166.1; 164.2; 156.2; 155.7; 151.1; 148.0; 144.4; 142.3; 130.4; 129.9 (2C); 124.0; 123.8; 123.2; 120.2; 119.0; 118.3 (2C); 116.1; 108.3; 103.5; 97.0; 85.9; 62.1; 53.9; 44.7 (2C); 12.3 (2C). HRMS (ESI, $[M+H]^+$) calculated for $C_{29}H_{29}N_4O_5$ 513.2138, found 513.2154. Purity (HPLC): 97.4% (t_R = 4.720 min, λ_{max} = 360 nm).

N-((1-(3-Hydroxy-4-phenoxybenzyl)-1H-1,2,3-triazol-4-yl)methyl)-2-oxo-2H-chromene-3-carboxamide (7e). General procedure for the azide-alkyne cycloaddition involving **5a** (50 mg, 0.208 mmol), alkyne **6e** (40 mg, 0.174 mmol), $CuSO_4.5H_2O$ (4.35 mg, 0.0174 mmol) and sodium ascorbate (14 mg, 0.070 mmol) in a mixture methanol (2 mL), water (7 mL) and dichloromethane (20 mL). Purification by flash chromatography (dichloromethane/methanol: 99/1) gave product **7e** as a white solid (70 mg, 86), R_f = 0.28 (dichloromethane/methanol: 97/3). ^{1}H NMR (DMSO-d_6, 500 MHz) δ 9.68 (s, 1H); 9.14 (t, *J* = 5.6 Hz, 1H); 8.89 (s, 1H); 8.06 (s, 1H); 8.00 (dd, *J* = 7.8 Hz, 1.5 Hz, 1H); 7.76 (ddd, *J* = 8.7, 7.0, 1.8 Hz, 1H); 7.51 (d, *J* = 8.4 Hz, 1H); 7.45 (ddd, *J* = 8.7 Hz, 7.1 Hz, 1.1 Hz, 1H); 7.31-7.27 (m, 2H); 7.01 (tt, *J* = 7.4, 1.0 Hz, 1H); 6.94 (d, *J* = 8.2 Hz, 1H); 6.89 (d, *J* = 2.1 Hz, 1H); 6.84-6.81 (m, 2H); 6.78 (dd, *J* = 8.2 Hz, 2.1 Hz, 1H); 5.51 (s, 2H); 4.60 (d, *J* = 5.6 Hz, 2H). ^{13}C NMR (DMSO-d_6, 126 MHz) δ 161.1; 160.3; 157.7; 153.9; 149.4; 147.7; 144.4; 142.4; 134.2; 133.1; 130.3; 129.6 (2C); 125.1; 123.1; 122.0; 121.9; 119.2; 118.8; 118.4; 116.7; 116.2 (2C); 116.2; 52.3; 34.9. HRMS (ESI, $[M+H]^+$) calculated for $C_{26}H_{21}N_4O_5$ 469.1512, found 469.1511. Purity (HPLC): > 99.9% (t_R = 2.886 min, λ_{max} = 300 nm).

7-(Diethylamino)-N-((1-(3-hydroxy-4-phenoxybenzyl)-1H-1,2,3-triazol-4-yl)methyl)-2-oxo-2H-chromene-3-carboxamide (7f). General procedure for the azide-alkyne cycloaddition involving azide **5a** (43 mg, 0.179 mmol), alkyne **6f** (44.6 mg, 0.15 mmol), $CuSO_4.5H_2O$ (3.8 mg, 0.015 mmol) and sodium ascorbate (12 mg, 0.06 mmol) in a mixture methanol (2 mL), water (5 mL) and dichloromethane (10 mL). Purification by flash chromatography (dichloromethane/methanol: 99/1) gave compound **7f** as a yellow solid (60 mg, 74%), R_f = 0.37 (dichloromethane/methanol: 99/1). ^{1}H NMR (DMSO-d_6, 500 MHz) δ 9.69 (bs, 1H); 9.05 (t, *J* = 5.6 Hz, 1H); 8.68 (s, 1H); 8.04 (s, 1H); 7.69 (d, *J* = 9.1 Hz, 1H); 7.31-7.28 (m, 2H); 7.00 (tt, *J* = 7.3, 1.0 Hz, 1H); 6.93 (d, *J* = 8.2 Hz, 1H); 6.89 (d, *J* = 2.0 Hz, 1H); 6.84-6.81 (m, 3H); 6.78 (dd, *J* = 8.3, 1.8 Hz, 1H); 6.61 (d, *J* = 2.0 Hz, 1H); 5.50 (s, 2H); 4.57 (d, *J* = 5.7 Hz, 2H); 3.48 (q, *J* = 7.0 Hz, 4H); 1.14 (t, *J* = 7.0 Hz, 6H). ^{13}C NMR (DMSO-d_6, 126 MHz) δ 162.2; 161.7; 157.7; 157.3; 152.5; 149.5; 147.9; 144.7; 142.4; 133.1; 131.6; 129.6 (2C); 123.0; 122.0; 121.9; 119.1; 116.7; 116.2 (2C); 110.2; 109.1; 107.6; 95.9; 52.3; 44.3; 34.7; 12.3; HRMS (ESI, $[M+H]^+$) calculated for $C_{30}H_{30}N_5O_5$ 540.2247, found 540.2240. Purity (HPLC): > 99.9% at 420 nm (t_R = 4.363 min).

N-((1-(3-Hydroxy-4-phenoxybenzyl)-1H-1,2,3-triazol-4-yl)methyl)-7-methoxy-2-oxo-2H-chromene-3-carboxamide (7g). General procedure for the azide-alkyne cycloaddition involving azide **5a** (9 mg, 0.037 mmol), alkyne **6g** (8 mg, 0.031 mmol), $CuSO_4.5H_2O$ (0.8 mg, 0.0031 mmol) and sodium ascorbate (2.5 mg, 0.0124 mmol) in a mixture methanol (0.5 mL), water (2.5 mL) and dichloromethane (6 mL). Purification by flash chromatography (dichloromethane/methanol: 98/2) gave product **7g** as a pale-yellow solid (13 mg, 87%), R_f = 0.14 (dichloromethane/methanol: 98/2). ^{1}H NMR (DMSO-d_6, 400 MHz) δ 9.67 (s, 1H); 9.08 (t, *J* = 5.6 Hz, 1H); 8.86 (s, 1H); 8.05 (s, 1H); 7.92 (d, *J* = 8.8 Hz, 1H); 7.31-7.27 (m, 2H); 7.12 (d, *J* = 2.2 Hz, 1H); 7.05 (dd, *J* = 8.7 Hz, 2.4 Hz, 1H); 7.01 (tt, *J* = 7.4, 1.0 Hz, 1H); 6.94 (d, *J* = 8.1 Hz, 1H); 6.89 (d, *J* = 2.1 Hz, 1H); 6.84-6.80 (m, 2H); 6.78 (dd, *J* = 8.1, 2.1 Hz, 1H); 5.51 (s, 2H); 4.59 (d, *J* = 5.6 Hz, 2H); 3.90 (s, 3H). ^{13}C NMR (DMSO-d_6, 126 MHz) δ 164.5; 161.4; 160.8; 157.7; 156.2; 149.4; 148.0; 144.5; 142.4; 133.1; 131.6; 129.6 (2C); 123.0; 122.0; 121.9; 119.2; 116.7; 116.2 (2C); 114.6; 113.7; 112.1; 100.3; 56.3; 52.3; 34.9. HRMS (ESI, $[M+H]^+$) calculated for $C_{27}H_{23}N_4O_6$ 499.1618, found 499.1626. Purity (HPLC): 95.4% at 350 nm (t_R = 3.367 min).

N-((1-(3-Hydroxy-4-phenoxybenzyl)-1H-1,2,3-triazol-4-yl)methyl)-8-methoxy-2-oxo-2H-chromene-3-carboxamide (7h). General procedure for the azide-alkyne cycloaddition involving azide **5a** (21.5 mg, 0.09 mmol), alkyne **6h** (19.3 mg, 0.075 mmol), $CuSO_4.5H_2O$ (1.9 mg, 0.0075 mmol) and sodium ascorbate (6 mg, 0.03 mmol) in a mixture methanol (1 mL), water (4 mL) and dichloromethane (10 mL). Purification by flash chromatography (dichloromethane/methanol: 98/2) gave product **7h** as a pale-yellow solid (22 mg, 59%), R_f = 0.08 (dichloromethane/methanol: 98/2). ^{1}H NMR (DMSO-d_6, 500 MHz) δ 9.67 (s, 1H); 9.14 (t, *J* = 5.6 Hz, 1H); 8.86 (s, 1H); 8.05 (s, 1H); 7.53 (dd, *J* = 8.0 Hz, 1.5 Hz, 1H); 7.44 (dd, *J* = 8.4, 1.4 Hz, 1H); 7.37 (dd, *J* = 8.2 Hz, 8.1 Hz, 1H); 7.31-7.27 (m, 2H); 7.01 (tt, *J* = 7.4, 1.0 Hz, 1H); 6.94 (d, *J* = 8.2 Hz, 1H); 6.89 (d, *J* = 2.1 Hz, 1H); 6.84-6.81 (m, 2H); 6.78 (dd, *J* = 8.1, 2.1 Hz, 1H); 5.51 (s, 2H); 4.59 (d, *J* = 5.5 Hz, 2H); 3.94 (s, 3H). ^{13}C NMR (DMSO-d_6, 126 MHz) δ 161.1; 160.0; 157.7; 149.4; 147.9; 146.3; 144.4; 143.2; 142.4; 133.1; 129.6 (2C); 125.1; 123.1; 122.0; 121.9; 121.2; 119.2; 119.0; 118.9; 116.7; 116.2 (2C); 116.1 56.2; 52.3; 34.9. HRMS (ESI, $[M+H]^+$) calculated for $C_{27}H_{23}N_4O_6$ 499.1618, found 499.1608. Purity (HPLC): 99.2% at 320 nm (t_R = 3.253 min).

6-Hydroxy-N-((1-(3-hydroxy-4-phenoxybenzyl)-1H-1,2,3-triazol-4-yl)methyl)-2-oxo-2H-chromene-4-carboxamide (7i). General procedure for the azide-alkyne cycloaddition involving azide **5a** (27 mg, 0.11 mmol), alkyne **6i** (25 mg, 0.096 mmol), $CuSO_4.5H_2O$ (2.4 mg, 0.0096 mmol) and sodium ascorbate (7.7 mg, 0.038 mmol) in a mixture methanol (1.1 mL), water (6.1 mL) and dichloromethane (10 mL). The mixture was filtered affording compound **7i** as a pale-yellow solid (27 mg, 48%), R_f = 0.08

(dichloromethane/methanol: 95/5). ^{1}H NMR (DMSO-d_6, 500 MHz) δ 9.94 (s, 1H); 9.67 (s, 1H); 9.17 (t, *J* = 5.6 Hz, 1H); 8.81 (s, 1H); 8.05 (s, 1H); 7.36 (d, *J* = 9.0 Hz, 1H); 7.31-7.27 (m, 3H); 7.18 (dd, *J* = 9.0, 2.8 Hz, 1H); 7.01 (tt, *J* = 7.4, 1.0 Hz, 1H); 6.93 (d, *J* = 8.2 Hz, 1H); 6.89 (d, *J* = 2.0 Hz, 1H); 6.84-6.81 (m, 2H); 6.77 (dd, *J* = 8.2 Hz, 2.0 Hz, 1H); 5.50 (s, 2H); 4.59 (d, *J* = 5.6 Hz, 2H). ^{13}C NMR (DMSO-d_6, 126 MHz) δ 161.3; 160.6; 157.7; 154.2; 149.4; 147.7; 147.4; 144.5; 142.4; 133.1; 129.6 (2C); 123.1; 122.5; 122.0; 121.9; 119.2; 119.0; 118.6; 117.1; 116.7; 116.2 (2C); 113.8; 52.3; 34.9. HRMS (ESI, $[M+H]^+$) calculated for $C_{26}H_{21}N_4O_6$ 485.1461, found 485.1449. Purity (HPLC): 96.5% at 290 nm (t_R = 2.108 min).

5-((4-(((7-Nitrobenzo[c][1,2,5]oxadiazol-4-yl)amino)methyl)-1H-1,2,3-triazol-1-yl)methyl)-2-phenoxyphenol (7j). General procedure for the azide-alkyne cycloaddition involving azide **5a** (50 mg, 0.208 mmol), alkyne **6j** (38 mg, 0.174 mmol), $CuSO_4.5H_2O$ (4.35 mg, 0.0174 mmol) and sodium ascorbate (14 mg, 0.070 mmol) in a mixture methanol (2 mL), water (7 mL) and dichloromethane (20 mL). The crude product was purified by flash chromatography (dichloromethane/methanol: 99/1) affording compound **7j** as an orange solid (32 mg, 44%), R_f = 0.15 (dichloromethane/methanol: 98/2). ^{1}H NMR (DMSO-d_6, 500 MHz) δ 9.85 (bs, 1H (H_{25})) ; 9.66 (bs, 1H); 8.52 (d, *J* = 8.9 Hz, 1H) ; 8.17 (s, 1H (H_{15})); 7.29 (t_{app}, *J* = 7.9 Hz, 2H); 7.01 (t, *J* = 7.3 Hz, 1H)); 6.92 (d, *J* = 8.1 Hz, 1H); 6.88 (d, *J* = 2.1 Hz, 1H); 6.81 (d, *J* = 8.2 Hz, 2H); 6.74 (dd, *J* = 8.2 Hz, 2.1 Hz, 1H) ; 6.53 (d, *J* = 8.9 Hz, 1H); 5.50 (s, 2H); 4.77 (s, 2H). ^{1}H NMR (DMSO-d_6, 126 MHz) δ 157.7; 149.3; 149.0; 143.8; 142.9; 141.8; 137.7; 142.5; 133.0; 129.6 (2C); 123.6; 122.1; 121.8; 119.2; 116.7; 116.3 (2C); 110.4; 99.9; 52.4; 38.6. HRMS (ESI, $[M+H]^+$) calculated for $C_{22}H_{18}N_7O_5$ 460.1369, found 460.1377. Purity (HPLC): 97.7% at 330 nm (t_R = 4.718 min).

7-(((1-(3-Hydroxy-4-phenoxybenzyl)-1H-1,2,3-triazol-4-yl)methyl)amino)-N,N-dimethylbenzo[c][1,2,5]oxadiazole-4-sulfonamide (7k). General procedure for the azide-alkyne cycloaddition involving azide **5a** (11.5 mg, 0.048 mmol), alkyne DBD **6k** (11 mg, 0.04 mmol), $CuSO_4.5H_2O$ (1.02 mg, 0.0041 mmol) and sodium ascorbate (3.3 mg, 0.0167 mmol) in a mixture methanol (1 mL), water (3.5 mL) and dichloromethane (10 mL). Purification by flash chromatography (dichloromethane/methanol: 98/2) gave compound **7k** as a yellow solid (15.5 mg, 75%), R_f = 0.12 (dichloromethane/methanol: 98/2). ^{1}H NMR (DMSO-d_6, 500 MHz) δ 9.71 (s, 1H); 8.77 (t, *J* = 5.6 Hz, 1H); 8.13 (s, 1H); 7.81 (d, *J* = 8.1 Hz, 1H); 7.30-7.27 (m, 2H) ; 7.01 (t, *J* = 7.4 Hz, 1H); 6.91 (d, *J* = 8.1 Hz, 1H); 6.87 (d, *J* = 2.0 Hz, 1H); 6.81 (d, *J* = 8.2 Hz, 2H); 6.73 (dd, *J* = 8.2, 2.0 Hz, 1H); 6.43 (d, *J* = 8.2 Hz, 1H); 5.48 (s, 2H); 4.66 (d, *J* = 5.5 Hz, 2H); 2.67 (s, 6H). ^{1}H NMR (DMSO-d_6, 126 MHz) δ 157.8; 149.4; 146.6; 144.5; 143.8; 142.6; 140.9; 140.4; 133.2; 129.8 (2C); 123.6; 122.3; 122.0; 119.3; 116.8; 116.4 (2C); 106.2; 99.7; 52.5; 38.4; 37.6 (2C). HRMS (ESI, $[M]^+$) calculated for $C_{24}H_{23}N_7O_5S$ 521.1481, found 521.1464. Purity (HPLC): > 99.9% at 420 nm (t_R = 3.235 min).

7-((1-(4-(2-Hydroxyphenoxy)benzyl)-1H-1,2,3-triazol-4-yl)methoxy)-2H-chromen-2-one (7l). General procedure for the azide-alkyne cycloaddition involving azide **5b** (50 mg, 0.208 mmol), alkyne **6i** (35 mg, 0.174 mmol), $CuSO_4.5H_2O$ (4.35 mg, 0.0174 mmol) and sodium ascorbate (14 mg, 0.696 mmol) in a mixture methanol (2 mL), water (7 mL) and dichloromethane (20 mL). Purification by flash chromatography gave compound **7l** as a white solid (80 mg, 87%), R_f = 0.17 (dichloromethane/methanol: 99/1). ^{1}H NMR (DMSO-d_6, 300 MHz) δ 9.52 (bs, 1H); 8.30 (s, 1H); 7.99 (d, *J* = 9.5 Hz, 1H); 7.63 (d, *J* = 8.6 Hz, 1H); 7.30 (d*, *J* = 8.8 Hz, 2H); 7.15 (d, *J* = 2.4 Hz, 1H) ; 7.05 (ddd, *J* = 8.7 Hz, 6.9 Hz, 1.7 Hz, 1H); 7.01 (dd, *J* = 8.6 Hz, 2.5 Hz, 1H); 6.96 (dd, *J* = 8.2 Hz, 1.6 Hz, 1H); 6.95 (dd, *J* = 8.2, 1.7 Hz, 1H); 6.83-6.79 (m, 3H); 6.30 (d, *J* = 9.5 Hz, 1H); 5.54 (s, 2H); 5.24 (2H). ^{13}C NMR (DMSO-d_6, 75 MHz) δ 161.1; 160.2; 158.0; 155.3; 149.4; 144.3; 142.2; 142.1; 129.7 (2C); 129.5; 129.2; 125.7; 124.7; 122.1; 119.7; 117.3; 116.1 (2C); 112.9; 112.7; 112.6; 101.6; 61.6; 52.3. HRMS (ESI, $[M+H]^+$) calculated for $C_{25}H_{20}N_3O_5$ 442.1403, found 442.1406. Purity (HPLC): 99.7% (t_R = 2.836 min, λ_{max} = 290 nm).

7-(Diethylamino)-N-((1-(4-(4-hexyl-2-hydroxyphenoxy)benzyl)-1H-1,2,3-triazol-4-yl)methyl)-2-oxo-2H-chromene-3-carboxamide (7m). General procedure for the azide-alkyne cycloaddition involving azide **5c** (24 mg, 0.07 mmol), alkyne **6f** (22 mg, 0.07 mmol), $CuSO_4.5H_2O$ (4 mg, 0.0146 mmol, 0.2 eq) and sodium ascorbate (6 mg, 0.03 mmol, 0.4 eq) in a mixture methanol (2 mL), water (5 mL) and dichloromethane (10 mL). Purification by flash chromatography (gradient dichloromethane/methanol: 100/0 to 95/5) gave compound **7m** as a pale-yellow solid (26 mg, 56%), R_f = 0.42 (dichloromethane/methanol: 95/05). ^{1}H NMR ($CDCl_3$, 600 MHz) δ 9.37 (s, 1H); 9.02 (t, *J* = 5.6 Hz, 1H); 8.67 (s, 1H); 7.99 (s, 1H); 7.69 (d, *J* = 9.1 Hz, 1H); 7.28 (d*, *J* = 8.8 Hz, 2H); 6.84 (d, *J* = 8.0 Hz, 1H); 6.81 (dd, *J* = 9.1 Hz, 2.5 Hz, 1H); 6.79 (d*, *J* = 8.7 Hz, 2H); 6.76 (d, *J* = 2.1 Hz, 1H); 6.62-6.60 (m, 3H); 5.48 (s, 2H); 4.53 (d, *J* = 5.6 Hz, 2H); 3.48 (q, *J* = 7.1 Hz, 4H); 2.53-2.48 (m, 2H); 1.53 (quint, *J* = 7.5 Hz, 2H); 1.31-1.23 (m, 6H); 1.14 (t, *J* = 7.1 Hz, 6H); 0.86 (t, *J* = 7.2 Hz, 3H). ^{13}C NMR ($CDCl_3$, 151 MHz) δ 162.2; 161.7; 158.2; 157.3; 152.5; 149.0; 147.9; 144.7; 139.9; 139.9; 131.6; 129.6 (2C); 129.1; 122.6; 121.9; 119.4; 117.1; 115.9 (2C); 110.2; 109.1; 107.6; 95.9; 52.2; 44.3; 34.7 (2C); 31.1; 30.8; 28.3; 22.0; 13.9; 12.3. HRMS (DCI-CH_4, $[M]^+$) calculated for $C_{36}H_{41}N_5O_5$ 623.3108, found: 623.3087. Purity (HPLC): > 99.9% at 420 nm (t_R = 6.393 min).

5-Hexyl-2-(4-((4-(((7-nitrobenzo[c][1,2,5]oxadiazol-4-yl)amino)methyl)-1H-1,2,3-triazol-1-yl)methyl)phenoxy)phenol (7n). General procedure for the azide-alkyne cycloaddition involving azide **5c** (13 mg, 0.04 mmol), alkyne **6k** (9 mg, 0.04 mmol), $CuSO_4.5H_2O$ (2 mg, 0.008 mmol, 0.2 eq) and

sodium ascorbate (3 mg, 0.015 mmol, 0.4 eq) in a mixture methanol (1.5 mL), water (4.5 mL) and dichloromethane (10 mL). Purification by flash chromatography (gradient dichloromethane/methanol: 100/0 to 95/5) gave compound **7n** as an orange solid (17 mg, 80%). R_f = 0.48 (dichloromethane/methanol: 95/5). ^{1}H NMR ($CDCl_3$, 600 MHz) δ 8.48 (d, *J* = 8.6 Hz, 1H); 7.50 (s, 1H); 7.25-7.24 (m, 2H); 6.99 (d*, *J* = 8.7 Hz, 2H); 6.88 (d, *J* = 2.1 Hz, 1H); 6.81 (d, *J* = 8.2 Hz, 2H); 6.69-6.67 (m, 2H); 6.35 (d, *J* = 8.6 Hz, 1H); 5.51 (s, 2H); 4.77 (d, *J* = 5.4 Hz, 2H); 2.56 (t, *J* = 7.9 Hz, 2H); 1.60-1.56 (m, 2H); 1.36-1.29 (m, 6H); 0.88 (t, *J* = 7.0 Hz, 3H). ^{13}C NMR ($CDCl_3$, 151 MHz) δ 158.1; 147.3; 144.3; 143.8; 142.9; 142.5; 141.0 140.1; 136.0; 129.9 (2C); 128.5; 125.1; 121.7; 120.8; 119.6 117.7 (2C); 116.4; 99.5; 53.9; 39.4; 35.5; 31.7; 31.3; 28.9; 22.6; 14.1. HRMS (DCI-CH_4, $[M+H]^+$) calculated for $C_{28}H_{30}N_7O_5$ 544.2308, found: 544.2316. Purity (HPLC): 95.8% at 330 nm (t_R = 6.205 min).

General procedure for the Ruthenium-catalysed azide-alkyne cycloaddition RuAAC [58]**.** A solution of azide **1e** (1 eq) and alkyne (1 eq) in degassed 1,4-dioxane ([alkyne] = 0.9 M) was added to a solution of Cp*RuCl(PPh_3)$_2$ (0.05 eq) in 1,4-dioxane ([Cp*RuCl(PPh_3)$_2$] = 0.009 M) under argon atmosphere. The mixture was stirred at 65 °C for 18h and the solvent was removed *in-vacuo.* Triazoles **5q, 5r** were obtained after purification by flash-chromatography.

7-((1-(3-hydroxy-4-phenoxybenzyl)-1H-1,2,3-triazol-5-yl)methoxy)naphthalen-2(1H)-one (8a). General procedure involving azide **2** (34.9 mg, 0.124 mmol), alkyne **6a** (24.9 mg, 0.124 mmol), Cp*RuCl(PPh_3)$_2$ (5.0 mg, 6.2 µmol, 0.05 eq) in degassed 1,4-dioxane (0.8 mL). The crude product was purified by flash chromatography (Gradient petroleum ether/ethyl acetate: 70/30 to 0/100) affording the expected compound as a beige solid (19.0 mg, 35%), R_f = 0.10 (petroleum ether/ethyl acetate: 40/60). ^{1}H NMR (DMSO-d_6, 600 MHz) δ 9.62 (s, 1H (H_{14})); 8.00 (d, *J* = 9.4 Hz, 1H (H_{22})); 7.95 (s, 1H (H_{16})); 7.65-7.60 (m, 1H (H_{25})); 7.31-7.27 (m ,2H ($H_{10,12}$)); 7.07 (d, *J* = 2.4 Hz, 1H (H_{19})); 7.01 (tt, *J* = 7.4, 1.0 Hz, 1H (H_{11})); 6.90 (d, *J* = 8.3 Hz, 1H (H_6)); 6.88 (dd, *J* = 8.6, 2.4 Hz, 1H (H_{26})); 6.82-6.80 (m, 2H ($H_{9,13}$)); 6.79 (d, *J* = 2.2 Hz, 1H (H_3)); 6.67 (dd, *J* = 8.2, 2.2 Hz, 1H (H_7)); 6.32 (d, *J* = 9.5 Hz, 1H (H_{23})); 5.62 (s, 2H (H_1)); 5.35 (s, 2H (H_{17})); ^{13}C NMR (DMSO-d_6, 151 MHz) δ 160.3 (C_{18}); 160.2 (C_{21}); 157.8 (C_8); 155.2 (C_{20}); 149.4 (C_4); 144.2 (C_{22}); 142.2 (C_5); 134.6 (C_{16}); 133.1 (C_{15}); 132.7 (C_2); 129.6 (2C, $C_{10,12}$); 129.5 (C_{25}); 122.0 (C_{11}); 121.8 (C_6); 118.8 (C_7); 116.2 (C_3); 116.2 (2C, $C_{9,13}$); 113.0 (C_{23}); 112.9 (C_{24}); 112.7 (C_{26}); 101.7 (C_{19}); 58.3 (C_{17}); 50.8 (C_1). HRMS (DCI-CH_4, $[M+H^+]$) for calculated for $C_{25}H_{19}N_3O_5$ 442.1403, found 442.1397. Purity (HPLC): 95.3% at 320 nm (t_R = 2.730 min).

7-((1-(3-hydroxy-4-phenoxybenzyl)-1H-1,2,3-triazol-5-yl)methoxy)-4-methylnaphthalen-2(1H)-one (8b). General involving azide **2** (30.8 mg, 0.124 mmol), alkyne **6b** (26.5 mg, 0.124 mmol),

$Cp^*RuCl(PPh_3)_2$ (4.9 mg, 6.2 µmol, 0.05 eq) in degassed 1,4-dioxane (0.8 mL). The crude product was purified by flash chromatography (Gradient petroleum ether/ethyl acetate: 70/30 to 0/100) affording the expected compound as a beige solid (16.4 mg, 29%), R_f = 0.11 (petroleum ether/ethyl acetate: 40/60). ^{1}H NMR (DMSO-d_6, 600 MHz) δ 9.62 (s, 1H (H_{14})); 7.95 (s, 1H (H_{16})); 7.67 (d, *J* = 8.9 Hz, 1H (H_{25})); 7.30-7.27 (m, 2H ($H_{10,12}$)); 7.06 (d, *J* = 2.5 Hz, 1H (H_{19})); 7.01 (tt, *J* = 7.4, 1.0 Hz, 1H (H_{11})); 6.91 (dd, *J* = 8.8, 2.2 Hz, 1H (H_{26})); 6.89 (d, *J* = 8.4 Hz, 1H (H_6)); 6.83-6.80 (m, 2H ($H_{9,13}$)); 6.79 (d, *J* = 2.2 Hz, 1H (H_3)); 6.67 (dd, *J* = 8.2, 2.2 Hz, 1H (H_7)); 6.27 (d, *J* = 1.3 Hz, 1H (H_{22})); 5.62 (s, 2H (H_1)); 5.36 (s, 2H (H_{17})); 2.39 (d, *J* = 1.3 Hz, 3H (H_{27})); ^{13}C NMR (DMSO-d_6, 151 MHz) δ 160.2 (C_{18}); 160.0 (C_{21}); 157.7 (C_8); 154.5 (C_{20}); 153.3 (C_{23}); 149.3 (C_4); 142.2 (C_5); 134.5 (C_{16}); 133.1 (C_{15}); 132.6 (C_2); 129.6 (2C, $C_{10,12}$); 126.5 (C_{25}); 122.0 (C_{11}); 121.8 (C_6); 118.8 (C_7); 116.2 (C_3); 116.2 (2C, $C_{9,13}$); 113.7 (C_{24}); 112.4 (C_{26}); 111.5 (C_{22}); 101.7 (C_{19}) 58.3 (C_{17}); 50.8 (C_1); 18.1 (C_{27}). HRMS (DCI-CH_4, [M+H$^+$]) for calculated for $C_{26}H_{22}N_3O_5$ 456.1481, found 456.1541.

4.2. Biology experimental

4.2.1. Molecular docking

Molecular graphics were performed with the UCSF Chimera package [59]. The protein structures were downloaded from the RCSB Protein Data Bank and aligned with MatchMaker [60] on a reference structure 1BVR (chain A, 1BVR:A) [19]. The protein structures, were prepared (structure checks, rotamers, hydrogenation, splitting of chains) using Biovia (www.3dsbiovia.com) Discovery Studio Visualizer 2021 (DSV), UCSF Chimera and in-house Python codes. Molecular modeling studies were carried with Molegro Virtual Docker 6 (www.molexus.com) software using 1P45 (chain A, 1P45:A) [9] and 2X22 (chain A, 2X22:A) [25] PDB entries as differential targets. The 1P45:A structure is characterized by a open major portal and a closed minor portal, in contrast to 2X22:A in which the major portal is closed and the minor portal is opened, the conformations of SBL (Substrate Binding Loop) extended region (residues 190-230) also differs, the structure of the cofactor (NAD^+) remains highly conserved. In addition to both enzyme conformations, two molecular docking protocols (MSE and OPT) and two internal scoring schemes (MolDock and ReRank) [61] were combined in a multimodal (docking) and consensus (scoring) approach. The two protocols share the same set of flexible residues: Ala154, Ala157, Ala164, Ala198, Ala201, Ala206, Arg195, Asn231, Asp148, Asp150, Gln214, Glu219, Ile202, Ile215, Leu217, Leu218, Lys165, Met98, Met103, Met155, Met161, Met199, Met232, Phe149, Phe97, Pro193, Thr162, Thr195, Trp160, Trp22, Tyr158. Softened potentials were used with a tolerance of 1 and a strength 0.9. According to structural studies, these residues cover different cases of minor and major portal fluctuations in InhA known structures. No displaceable water molecules were taken

in account inner the binding site (known as mainly hydrophobic). The corresponding NAD molecules (from 1P45:A or 2X22:A) were treated as cofactors and where set as NAD^+ with partial negative charges on phosphates and positive charge on nicotinamide group. The NAD is not flexible during the docking process, but treated independently of the protein: a component Ligand-Cofactor (in addition to the Ligand-Protein contribution) was used in docking scores calculations. Clustering of poses (tabu clustering) was set with an RMS threshold of 1.9 Å in order to be a little more discriminant on the best poses. Templates (pharmacophoric profile) were used with a strength of -500 and a grid resolution of 0.4 Å using conserved atom positions along InhA ligands: ether group (oxygen, hydrogen donor); alcohol group (oxygen, hydrogen donor/acceptor) and ring (carbons) of ligand TCU (PT70, taken from 2X22:A), similarity measure parameters were let at their default values. In the case of OPT (Differential evolution algorithm) protocol, the docking process used 10000 iteration steps, and a grid resolution of 0.3 Å, along 40 (1P45:A) or 30 (2X22:A) independent runs. The convergence was reached for all ligands, internal parameters (population size, crossover rate, scaling factor...) of the algorithm were let as default. A final minimization (per run) was parameterized using 4000 steps for lateral chains and 2000 steps for protein backbone followed by a minimization and optimization (hydrogen bonds) of ligands. The same parameters were applied to the MSE (Simplex evolution algorithm) protocol, internal parameters (population size, number of iterations, energy threshold...) of the algorithm were let as default. The docking parameters used for all these simulations were benchmarked for their ability to reproduce the conformation of several co-crystalized inhibitors such TCL in 1P45:A and TCU in 2X22:A. Typical root-mean-square deviation (RMSD) between the docking poses and X-ray structures were in the range 0.5-1.0 Å for the best poses (ReRank and MolDock combined scores). The most realistic complexes (best poses) were selected on the basis of conformity and strength. Conformity reflects the ability to reproduce the conformation of TCL-based ligands bound to InhA in known X-ray crystal structures complexes and the corresponding interaction network, mainly π-π or π-alkyl interactions with nicotinamide group of NAD, hydrogen bonding with Tyr158, hydrogen or electrostatic interactions with cofactor (OH from ribose, amido group, phosphates, charged nitrogen of pyridinium). If a given pose is found to be in the best group of values for both docking scores (ReRank and MolDock), this pose is qualified as strong.

4.2.2. Production and purification of InhA

Optimized InhA sequence from Mtb (UniProt P9WGR1) for *Escherichia coli* BL21(DE3) strain with GenSmart™ Codon Optimization tool (Genscript) was inserted in pET15b plasmid using NdeI and BamHI restriction sites. A colony from transformed BL21(DE3) with the pET15b-InhA plasmid was grown in LB medium containing 100 µg/mL ampicillin at 37 °C 180 rpm overnight. 10 mL of this culture

was added to 990 mL LB medium containing ampicillin (100 µg/mL) and incubated at 37 °C 150 rpm until an optical density (OD) at 600 nm of 0.6-0.8 was reached. Then, 1 mL of isopropyl-β-D-1-thiogalactopyranoside (IPTG) 1 M was added before incubating the bacteria for 4 h at 150 rpm at 30 °C. Bacteria cells were pelleted by centrifugation at 6,000×*g* for 30 min at 4 °C, then resuspended with buffer A (20 mM Tris-HCl, 300 mM NaCl, 10 mM imidazole, pH 7.9) and lysed using an Emulsiflex-C5 cell disruptor (Avestin). After a centrifugation at 25,000×*g* for 30 min at 4 °C, the supernatant was filtered off with a 0.2 µm filter and injected into a nickel-chelated HisTrap HP column (Cytiva) equilibrated with buffer A. Unbound proteins were washed off with buffer A, then His_6-InhA was eluted using buffer 20 mM Tris-HCl, 300 mM NaCl, 300 mM imidazole, pH 7.9. Fractions containing His_6-InhA were pooled together and concentrated.

For enzymatic assays, the concentrated protein was centrifuged at 10,000×*g* for 10 minutes at 4 °C and injected into a preparative gel filtration SepFast 16/60 6-600 kDa pg column (BioToolomics) pre-equilibrated with buffer 30 mM PIPES, 150 mM NaCl, pH 6.8. His_6-InhA containing fractions were flash frozen in liquid nitrogen at a final concentration of 5 µM.

For crystallographic assays, concentrated His_6-InhA from affinity purification was incubated at room temperature with Thrombin (Novagen) overnight to cleave the histidine tag. Then, the solution was filtered off with a 0.2 µm filter and injected again into a nickel-chelated HisTrap HP column (Cytiva) equilibrated with buffer A and cleaved proteins were eluted with the same buffer. Fractions corresponding to the cleaved InhA were pooled together, concentrated, centrifuged at 10,000×*g* for 10 min at 4 °C and injected on a preparative gel filtration column SepFast 16/60 6-600 kDa pg column (BioToolomics) equilibrated with buffer 30 mM PIPES, 150 mM NaCl, pH 6.8. Fractions corresponding to InhA were collected and concentrated.

4.2.3. Evaluation of InhA enzyme inhibition

NADH was obtained from Sigma-Aldrich. Stock solutions of all compounds were prepared in DMSO (5% v/v). Kinetic assays were performed using *trans*-2-dodecenoyl-coenzyme A (DDCoA) and His_6-InhA as previously described [62]. Briefly, reactions were performed at 25 °C in 30 mM PIPES, 150 mM NaCl, pH 6.8 containing 250 µM of the NADH cofactor, 50 µM of the DDCoA substrate and the tested compound at different concentrations. Reactions were initiated by addition of InhA (50 nM final) and NADH oxidation was followed at 340 nm. The inhibitory activity of each compound was expressed as the percentage of inhibition of the InhA activity (initial velocity of the reaction) with respect to the control reaction without inhibitor. Inhibition = ((Slope InhA alone – slope with compound) / Slope InhA alone)*100. All activity assays were performed in duplicate or triplicate. IC_{50} values were determined using the 4-parameter curve-fitting software XLFit (IDBS) with at least six points.

4.2.4. Crystallization and structure determination

To obtain crystals of InhA in complex with ligands, cleaved InhA (in 30 mM PIPES, 150 mM NaCl, pH 6.8) was co-incubated at either 4 or 8 mg/mL with NAD^+ (respectively 1.4 and 2.8 mM, corresponding to a 1:10 protein/NAD^+ ratio) for 1 h at 4 °C. Mixtures were then placed at room temperature 10 min before adding ligands (solubilized in DMSO), by respecting the final 5% v/v DMSO with the protein. After 2 h incubation at room temperature or 4 °C, depending on the ligand solubility, crystallization assays were performed using the vapor diffusion method at 20 °C by mixing, with the help of a Mosquito crystallization robot (SPT Labtech, Melbourn, UK), 200 nL of InhA previously incubated with NAD^+ and ligands with 200 nL of reservoir solution containing 14% PEG 4000, 100 mM ADA, 100 mM ammonium acetate, 5 % v/v DMSO, pH 6.8. After 1 week, crystals were cryoprotected with paraffine before being flash frozen in liquid nitrogen. Diffraction data were collected at the ESRF beamline ID30B and the ALBA beamline XALOC, processed with autoProc [63], staraniso [64], and XDS [65] **(Supporting Information Table S1)**. Structures were solved by molecular replacement with MOLREP [66] using the A chain of 4OHU in the case of the complex in the presence of **7b** and 4OYR in the case of **7e**. Refinement was performed using Buster/TNT [67]. Dictionaries for compounds were generated using Grade2 [68] and used in Coot (0.9.8.1) for model building [69].

4.2.5. Inhibition of mycobacterial growth

Colorimetric microassay based on the reduction of tetrazolium salts (MTT, Thiazolyl Blue Tetrazolium Bromide, Sigma) to formazan by metabolically active mycobacteria was used to measure the susceptibility of Mtb H37Rv to each molecule by determining its minimum inhibitory concentration (MIC) as previously described [70]. Briefly, bacterial cells growing as surface pellicle were recovered from 100 mL culture in 7H9 broth (Middlebrook 7H9 broth base BD Difco) containing 0.2% glycerol (w/v), vortexed with 4 mm glass beads, suspended in 20 mL 7H9 broth-0.2% glycerol and centrifuged at 800 rpm to eliminate residual clumps. Serial twofold dilutions of each compound to be tested (stock solution at 1 or 10 mM in DMSO) were prepared in 100 µL 7H9 broth using 96-well flat bottom microplates (Nunc). 100 µl of mycobacterial suspension (OD 600 nm 0.1) in 7H9 broth were then added to each well. After 6 days incubation at 37 °C, MTT was added (50 µl at 1 mg/ml). After one-day incubation at 37 °C, 50 µL of 20% SDS solution were added to each well to solubilize formazan crystals and the OD of each well was measured at 570 nm (microplate reader Expert plus 96, ASYS HITECH, Austria). The MIC was determined as the lowest concentration of drug that inhibited bacterial growth

from at least three independent experiments. The data were normalized to the value measured in untreated wells, after subtracting the background absorbance to each value.

4.2.6. Inhibition of mycolic acid biosynthesis

Mtb H37Rv cells were cultivated in 7H9 broth with albumin-dextrose-catalase and 0.05% Tween 80 at 37 °C with shaking (120 rpm). **INH** and compounds **7b**, **7d** and **7n** (at final concentrations of 0, 1×, 5× and 25× their MICs, stock in DMSO) were added when the culture reached O.D (600 nm) ~ 0.2. At the same time, the ^{14}C-acetate (specific activity 110 mCi/mmol, ARC) was added at final concentration of 0.5 μCi/mL. After 24 h of static cultivation at 37 °C, the cultures were harvested and the fatty/mycolic acids were extracted from whole cells from 100 μL cultures and derivatized to corresponding methyl esters (FAME/MAME) [71]. Dried extracts were dissolved in 50 μL of chloroform/methanol (2:1, v/v) and 5 μL were loaded on TLC silica gel 60 F254 plates (Merck). FAME/MAME were separated in n-hexane/ethyl acetate (95:5, 3 runs) and visualized using an AmershamTM TyphoonTM Biomolecular Imager.

Lipids were extracted from cells from 100 μL cultures containing the same concentrations of compounds with 1.5 mL chloroform/methanol (2 :1 v/v) at 65 °C for 2 h. Then 150 μl of H_2O were added, the samples were mixed, centrifuged and bottom organic phases were removed and dried under N_2. Lipid extracts were subjected to biphasic Folch washing. Isolated lipids were dissolved in 30 μL of chloroform/methanol (2: 1, v/v) and 5 μL were loaded on the thin-layer chromatography (TLC) silica gel plates F254 (Merck). Lipids were separated in chloroform/methanol/water (20:4:0.5, v/v/v) and visualized using an AmershamTM TyphoonTM Biomolecular Imager.

4.2.7. Analysis of sensitivity of Mtb H37Ra strains overproducing KatG/InhA/HadABC

InhA protein, HadABC complex and $KatG_{smeg}$ protein encoded by the gene *msmeg_6384* from *M. smegmatis* were overproduced in Mtb H37Ra using pMV261-*inhA*, pVV16-*hadABC* or pVV16-*katG*$_{smeg}$ constructs as already described [72-74]. Sensitivity of Mtb H37Ra strains overproducing InhA, HadABC and $KatG_{smeg}$, as well as control strains carrying empty pMV261 and pVV16 vectors, to compounds **7b**, **7d**, and **7n** was analyzed by drop dilution method. The culture of each strain was diluted to OD (600 nm) = 0.5. Then, 4 μl of 1x, 10x and 100x diluted samples were plated on 7H11-agar + 10 % oleic acid-albumin-dextrose-catalase containing various concentrations of tested compounds **7b** and **7d** (0.625, 1.25, 6.25, 12.5, 25 μM) and **7n** (1.25, 2.5, 12.5, 25, 50 μM). Plates were incubated for 18 days at 37 °C.

4.2.8. Cell viability assays

Human cell lines were grown at 37 °C in a humidified 5 % CO_2 incubator in DMEM high-glucose (Thermo Fisher Scientific) for HCT116 (Horizon Discovery), MEM containing Earle's salts, sodium pyruvate and non-essential amino acids for CACO2 (DSMZ), HepG2 (ATCC) and WI38hTERT (generous gift from Dr Olivier Sordet, CRCT, Toulouse). All media contained 10 % or 20 % (for CACO2) fetal bovine serum (Eurobio), 2.5 mM L-glutamine, 100 U/mL penicillin and 100 µg/mL streptomycin. For SRB assays, cells were plated in 96-well plates (Nunc Edge) at 1500, 2500, 9000 and 3500 cells/well respectively for HCT116, CACO2, HepG2 and WI38hTERT 24 h before treatment with the drug. Serial 2-fold dilutions were performed in medium and used to treat cells for 72 h. At the end of treatment, cells were fixed and stained with SRB as described [75]. After resuspending the dye in a 10 mM Tris-base solution, the OD at 490 nm of each well was measured (µQuant plate reader, Bio-tek) as a readout of the cell number. For calculation, background absorbance was subtracted to each value and the data were normalized to the value measured in untreated wells. Each point was measured in duplicate and the IC50 were computed from at least three independent experiments using the GraphPad Prism software to perform a non-linear regression to a four-parameter logistic curve (Inhibitor vs response; variable slope). An approximate value was provided when the curve did not fit the logistic curve.

Acknowledgments

We thank the mass spectrometry service, Institut de Chimie de Toulouse ICT-UAR 2599 (Université de Toulouse, CNRS, Toulouse, France, https://ict.cnrs.fr) for help with chemical analyses. We thank Isabelle Fabing for her help with chromatographic analyses and purification. We also thank the scientific staff of the European Synchrotron Radiation Facility (Grenoble, France), SOLEIL (Gif sur Yvette, France) and ALBA (Barcelona, Spain). We particularly thank the staff of beamlines XALOC at ALBA and ID30B at the European Synchrotron Radiation Facility, where the crystallographic experiments were conducted. We also thank Valérie Guillet for managing synchrotron radiation trips. The UPLC, UPC2, crystallization and macromolecular crystallography equipment used in this study are part of the Integrated Screening Platform of Toulouse (PICT, IBiSA). We thank Williams R. Jacobs, Jr. for pMV261-*inhA* construct and Mary Jackson for pVV16-*hadABC* construct. We thank Stéphanie Ballereau for giving us a sample of DBD-Cl, precursor of compound **6k**. This work was supported by Slovak Research and Development Agency (grant n. APVV-19-0189), and by the OPII, ACCORD, ITMS2014+: 313021X329, co-financed by ERDF. This study received funding from the l'Université

Fédérale de Toulouse Midi-Pyrénées (UFTMiP) and the Région Occitanie for a PhD grant (R. Tamhaev) and the Région Occitanie for a “Pré-maturation Prostacure” grant to S. Britton and N. Preuilh.

References

[1] WHO, Global Tuberculosis Report 2022, in, World Health Organization, Geneva, 2022.
[2] A. Banerjee, E. Dubnau, A. Quemard, V. Balasubramanian, K.S. Um, T. Wilson, D. Collins, G. de Lisle, W.R. Jacobs, Jr., inhA, a gene encoding a target for isoniazid and ethionamide in Mycobacterium tuberculosis, Science, 263 (1994) 227-230.
[3] S.L. Parikh, G. Xiao, P.J. Tonge, Inhibition of InhA, the enoyl reductase from Mycobacterium tuberculosis, by triclosan and isoniazid, Biochemistry, 39 (2000) 7645-7650.
[4] M.E. Boyne, T.J. Sullivan, C.W. amEnde, H. Lu, V. Gruppo, D. Heaslip, A.G. Amin, D. Chatterjee, A. Lenaerts, P.J. Tonge, R.A. Slayden, Targeting fatty acid biosynthesis for the development of novel chemotherapeutics against Mycobacterium tuberculosis: evaluation of A-ring-modified diphenyl ethers as high-affinity InhA inhibitors, Antimicrobial agents and chemotherapy, 51 (2007) 3562-3567.
[5] P. Pan, S.E. Knudson, G.R. Bommineni, H.J. Li, C.T. Lai, N. Liu, M. Garcia-Diaz, C. Simmerling, S.S. Patil, R.A. Slayden, P.J. Tonge, Time-dependent diaryl ether inhibitors of InhA: structure-activity relationship studies of enzyme inhibition, antibacterial activity, and in vivo efficacy, ChemMedChem, 9 (2014) 776-791.
[6] F. Rodriguez, N. Saffon, J.C. Sammartino, G. Degiacomi, M.R. Pasca, C. Lherbet, First triclosan-based macrocyclic inhibitors of InhA enzyme, Bioorg Chem, 95 (2020) 103498.
[7] J. Stec, C. Vilcheze, S. Lun, A.L. Perryman, X. Wang, J.S. Freundlich, W. Bishai, W.R. Jacobs, Jr., A.P. Kozikowski, Biological evaluation of potent triclosan-derived inhibitors of the enoyl-acyl carrier protein reductase InhA in drug-sensitive and drug-resistant strains of Mycobacterium tuberculosis, ChemMedChem, 9 (2014) 2528-2537.
[8] A. Chollet, G. Mori, C. Menendez, F. Rodriguez, I. Fabing, M.R. Pasca, J. Madacki, J. Kordulakova, P. Constant, A. Quemard, V. Bernardes-Genisson, C. Lherbet, M. Baltas, Design, synthesis and evaluation of new GEQ derivatives as inhibitors of InhA enzyme and Mycobacterium tuberculosis growth, Eur J Med Chem, 101 (2015) 218-235.
[9] M.R. Kuo, H.R. Morbidoni, D. Alland, S.F. Sneddon, B.B. Gourlie, M.M. Staveski, M. Leonard, J.S. Gregory, A.D. Janjigian, C. Yee, J.M. Musser, B. Kreiswirth, H. Iwamoto, R. Perozzo, W.R. Jacobs, Jr., J.C. Sacchettini, D.A. Fidock, Targeting tuberculosis and malaria through inhibition of Enoyl reductase: compound activity and structural data, J Biol Chem, 278 (2003) 20851-20859.
[10] A. Suresh, S. Srinivasarao, N. Agnieszka, A.K. Ewa, M. Alvala, C. Lherbet, K.V.G. Chandra Sekhar, Design and synthesis of 9H-fluorenone based 1,2,3-triazole analogues as Mycobacterium tuberculosis InhA inhibitors, Chem Biol Drug Des, 91 (2018) 1078-1086.
[11] P.S. Shirude, P. Madhavapeddi, M. Naik, K. Murugan, V. Shinde, R. Nandishaiah, J. Bhat, A. Kumar, S. Hameed, G. Holdgate, G. Davies, H. McMiken, N. Hegde, A. Ambady, J. Venkatraman, M. Panda, B. Bandodkar, V.K. Sambandamurthy, J.A. Read, Methyl-thiazoles: a novel mode of inhibition with the potential to develop novel inhibitors targeting InhA in Mycobacterium tuberculosis, J Med Chem, 56 (2013) 8533-8542.
[12] R.C. Hartkoorn, C. Sala, J. Neres, F. Pojer, S. Magnet, R. Mukherjee, S. Uplekar, S. Boy-Rottger, K.H. Altmann, S.T. Cole, Towards a new tuberculosis drug: pyridomycin - nature's isoniazid, EMBO Mol Med, 4 (2012) 1032-1042.
[13] M. Kienle, P. Eisenring, B. Stoessel, O.P. Horlacher, S. Hasler, G. van Colen, R.C. Hartkoorn, A. Vocat, S.T. Cole, K.H. Altmann, Synthesis and Structure-Activity Relationship Studies of C2-Modified Analogs of the Antimycobacterial Natural Product Pyridomycin, J Med Chem, 63 (2020) 1105-1131.
[14] U.H. Manjunatha, S.P.S. Rao, R.R. Kondreddi, C.G. Noble, L.R. Camacho, B.H. Tan, S.H. Ng, P.S. Ng, N.L. Ma, S.B. Lakshminarayana, M. Herve, S.W. Barnes, W. Yu, K. Kuhen, F. Blasco, D. Beer, J.R. Walker, P.J. Tonge, R. Glynne, P.W. Smith, T.T. Diagana, Direct inhibitors of InhA are active against Mycobacterium tuberculosis, Sci Transl Med, 7 (2015) 269ra263.

[15] M. Martinez-Hoyos, E. Perez-Herran, G. Gulten, L. Encinas, D. Alvarez-Gomez, E. Alvarez, S. Ferrer-Bazaga, A. Garcia-Perez, F. Ortega, I. Angulo-Barturen, J. Rullas-Trincado, D. Blanco Ruano, P. Torres, P. Castaneda, S. Huss, R. Fernandez Menendez, S. Gonzalez Del Valle, L. Ballell, D. Barros, S. Modha, N. Dhar, F. Signorino-Gelo, J.D. McKinney, J.F. Garcia-Bustos, J.L. Lavandera, J.C. Sacchettini, M.S. Jimenez, N. Martin-Casabona, J. Castro-Pichel, A. Mendoza-Losana, Antitubercular drugs for an old target: GSK693 as a promising InhA direct inhibitor, EBioMedicine, 8 (2016) 291-301.
[16] Y. Xia, Y. Zhou, D.S. Carter, M.B. McNeil, W. Choi, J. Halladay, P.W. Berry, W. Mao, V. Hernandez, T. O'Malley, A. Korkegian, B. Sunde, L. Flint, L.K. Woolhiser, M.S. Scherman, V. Gruppo, C. Hastings, G.T. Robertson, T.R. Ioerger, J. Sacchettini, P.J. Tonge, A.J. Lenaerts, T. Parish, M. Alley, Discovery of a cofactor-independent inhibitor of Mycobacterium tuberculosis InhA, Life Sci Alliance, 1 (2018) e201800025.
[17] A. Dessen, A. Quemard, J.S. Blanchard, W.R. Jacobs, Jr., J.C. Sacchettini, Crystal structure and function of the isoniazid target of Mycobacterium tuberculosis, Science, 267 (1995) 1638-1641.
[18] A. Chollet, L. Maveyraud, C. Lherbet, V. Bernardes-Genisson, An overview on crystal structures of InhA protein: Apo-form, in complex with its natural ligands and inhibitors, Eur J Med Chem, 146 (2018) 318-343.
[19] D.A. Rozwarski, C. Vilchèze, M. Sugantino, R. Bittman, J.C. Sacchettini, Crystal structure of the Mycobacterium tuberculosis enoyl-ACP reductase, InhA, in complex with NAD+ and a C16 fatty acyl substrate, J Biol Chem, 274 (1999) 15582-15589.
[20] T.J. Sullivan, J.J. Truglio, M.E. Boyne, P. Novichenok, X. Zhang, C.F. Stratton, H.J. Li, T. Kaur, A. Amin, F. Johnson, R.A. Slayden, C. Kisker, P.J. Tonge, High affinity InhA inhibitors with activity against drug-resistant strains of Mycobacterium tuberculosis, ACS Chem Biol, 1 (2006) 43-53.
[21] H.J. Li, C.T. Lai, P. Pan, W. Yu, N. Liu, G.R. Bommineni, M. Garcia-Diaz, C. Simmerling, P.J. Tonge, A structural and energetic model for the slow-onset inhibition of the Mycobacterium tuberculosis enoyl-ACP reductase InhA, ACS Chem Biol, 9 (2014) 986-993.
[22] P. Kamsri, C. Hanwarinroj, N. Phusi, T. Pornprom, K. Chayajarus, A. Punkvang, N. Suttipanta, P. Srimanote, K. Suttisintong, C. Songsiriritthigul, P. Saparpakorn, S. Hannongbua, S. Rattanabunyong, S. Seetaha, K. Choowongkomon, S. Sureram, P. Kittakoop, P. Hongmanee, P. Santanirand, Z. Chen, W. Zhu, R.A. Blood, Y. Takebayashi, P. Hinchliffe, A.J. Mulholland, J. Spencer, P. Pungpo, Discovery of New and Potent InhA Inhibitors as Antituberculosis Agents: Structure-Based Virtual Screening Validated by Biological Assays and X-ray Crystallography, Journal of Chemical Information and Modeling, 60 (2020) 226-234.
[23] J.S. Freundlich, F. Wang, C. Vilchèze, G. Gulten, R. Langley, G.A. Schiehser, D.P. Jacobus, W.R. Jacobs Jr., J.C. Sacchettini, Triclosan Derivatives: Towards Potent Inhibitors of Drug-Sensitive and Drug-Resistant Mycobacterium tuberculosis, ChemMedChem, 4 (2009) 241-248.
[24] C.-T. Lai, H.-J. Li, W. Yu, S. Shah, G.R. Bommineni, V. Perrone, M. Garcia-Diaz, P.J. Tonge, C. Simmerling, Rational Modulation of the Induced-Fit Conformational Change for Slow-Onset Inhibition in Mycobacterium tuberculosis InhA, Biochemistry, 54 (2015) 4683-4691.
[25] S.R. Luckner, N. Liu, C.W. am Ende, P.J. Tonge, C. Kisker, A slow, tight binding inhibitor of InhA, the enoyl-acyl carrier protein reductase from Mycobacterium tuberculosis, J Biol Chem, 285 (2010) 14330-14337.
[26] H.H. Soutter, P. Centrella, M.A. Clark, J.W. Cuozzo, C.E. Dumelin, M.A. Guie, S. Habeshian, A.D. Keefe, K.M. Kennedy, E.A. Sigel, D.M. Troast, Y. Zhang, A.D. Ferguson, G. Davies, E.R. Stead, J. Breed, P. Madhavapeddi, J.A. Read, Discovery of cofactor-specific, bactericidal Mycobacterium tuberculosis InhA inhibitors using DNA-encoded library technology, Proceedings of the National Academy of Sciences of the United States of America, 113 (2016) E7880-e7889.
[27] L.A. Spagnuolo, S. Eltschkner, W. Yu, F. Daryaee, S. Davoodi, S.E. Knudson, E.K. Allen, J. Merino, A. Pschibul, B. Moree, N. Thivalapill, J.J. Truglio, J. Salafsky, R.A. Slayden, C. Kisker, P.J. Tonge, Evaluating the Contribution of Transition-State Destabilization to Changes in the Residence Time of Triazole-Based InhA Inhibitors, J Am Chem Soc, 139 (2017) 3417-3429.
[28] L.-Y. Ma, Y.-C. Zheng, S.-Q. Wang, B. Wang, Z.-R. Wang, L.-P. Pang, M. Zhang, J.-W. Wang, L. Ding, J. Li, C. Wang, B. Hu, Y. Liu, X.-D. Zhang, J.-J. Wang, Z.-J. Wang, W. Zhao, H.-M. Liu, Design, Synthesis,

and Structure–Activity Relationship of Novel LSD1 Inhibitors Based on Pyrimidine–Thiourea Hybrids As Potent, Orally Active Antitumor Agents, Journal of Medicinal Chemistry, 58 (2015) 1705-1716.
[29] S. Bhakta, N. Scalacci, A. Maitra, A.K. Brown, S. Dasugari, D. Evangelopoulos, T.D. McHugh, P.N. Mortazavi, A. Twist, E. Petricci, F. Manetti, D. Castagnolo, Design and Synthesis of 1-((1,5-Bis(4-chlorophenyl)-2-methyl-1H-pyrrol-3-yl)methyl)-4-methylpiperazine (BM212) and N-Adamantan-2-yl-N'-((E)-3,7-dimethylocta-2,6-dienyl)ethane-1,2-diamine (SQ109) Pyrrole Hybrid Derivatives: Discovery of Potent Antitubercular Agents Effective against Multidrug-Resistant Mycobacteria, Journal of Medicinal Chemistry, 59 (2016) 2780-2793.
[30] O.A. Abdelaziz, D.I.A. Othman, M.M. Abdel-Aziz, S.M.I. Badr, H.M. Eisa, Novel diaryl ether derivatives as InhA inhibitors: Design, synthesis and antimycobacterial activity, Bioorganic Chemistry, 129 (2022).
[31] T.S. Ibrahim, E.S. Tahe, E. Samir, A.M. Malebar, A.N. Khayya, M.F.A. Mohamed, R.M. Bokhti, M.A. AlAwad, I.A. Seliem, H.Z. Asfou, N.A. Alhakamy, S.S. Panda, A.M.M. Al-Mahmoudy, In vitro antimycobacterial activity and physicochemical characterization of diaryl ether triclosan analogues as potential inhA reductase inhibitors, Molecules, 25 (2020).
[32] F. Rodriguez, N. Saffon, J.C. Sammartino, G. Degiacomi, M.R. Pasca, C. Lherbet, First triclosan-based macrocyclic inhibitors of InhA enzyme, Bioorganic Chemistry, 95 (2020).
[33] A.P. Tiwari, B. Sridhar, H.I. Boshoff, K. Arora, G. Gautham Shenoy, K.E. Vandana, G. Varadaraj Bhat, Design, synthesis, in silico and in vitro evaluation of novel diphenyl ether derivatives as potential antitubercular agents, Molecular Diversity, 24 (2020) 1265-1279.
[34] R. Vosatka, M. Kratky, J. Vinsova, Triclosan and its derivatives as antimycobacterial active agents, Eur J Pharm Sci, 114 (2018) 318-331.
[35] S. Chetty, T. Armstrong, S. Sharma Kharkwal, W.C. Drewe, C.I. De Matteis, D. Evangelopoulos, S. Bhakta, N.R. Thomas, New InhA Inhibitors Based on Expanded Triclosan and Di-Triclosan Analogues to Develop a New Treatment for Tuberculosis, Pharmaceuticals (Basel), 14 (2021).
[36] H. Liu, D.-G. Xia, Z.-W. Chu, R. Hu, X. Cheng, X.-H. Lv, Novel coumarin-thiazolyl ester derivatives as potential DNA gyrase Inhibitors: Design, synthesis, and antibacterial activity, Bioorganic Chemistry, 100 (2020) 103907.
[37] L. Xu, J. Yu, L. Jin, L. Pan, Design, Synthesis, and Antifungal Activity of 4-Amino Coumarin Based Derivatives, Molecules, 27 (2022).
[38] Y. Yun, J. Yang, Y. Miao, X. Wang, J. Sun, Synthesis and biological evaluation of 4-arylcoumarins as potential anti-Alzheimer's disease agents, Bioorganic & Medicinal Chemistry Letters, 30 (2020) 126900.
[39] R. Martinčič, J. Mravljak, U. Švajger, A. Perdih, M. Anderluh, M. Novič, In Silico Discovery of Novel Potent Antioxidants on the Basis of Pulvinic Acid and Coumarine Derivatives and Their Experimental Evaluation, PloS one, 10 (2015) e0140602.
[40] L. Rubab, S. Afroz, S. Ahmad, S. Hussain, I. Nawaz, A. Irfan, F. Batool, K. Kotwica-Mojzych, M. Mojzych, An Update on Synthesis of Coumarin Sulfonamides as Enzyme Inhibitors and Anticancer Agents, in: Molecules, 2022.
[41] Q.-H. Cui, W.-B. Li, Z.-Y. Wang, K.-Y. Xu, S. Wang, J.-T. Shi, L.-W. Zhang, S.-W. Chen, Design, synthesis and biological evaluation of coumarin derivatives as potential BRD4 inhibitors, Bioorganic Chemistry, 128 (2022) 106117.
[42] S.M. Somagond, R.R. Kamble, P.K. Bayannavar, S.K.J. Shaikh, S.D. Joshi, V.M. Kumbar, A.R. Nesaragi, M.Y. Kariduraganavar, Click chemistry based regioselective one-pot synthesis of coumarin-3-yl-methyl-1,2,3-triazolyl-1,2,4-triazol-3(4H)-ones as newer potent antitubercular agents, Archiv der Pharmazie, 352 (2019) e1900013.
[43] S. Srivastava, D. Bimal, K. Bohra, B. Singh, P. Ponnan, R. Jain, M. Varma-Basil, J. Maity, M. Thirumal, A.K. Prasad, Synthesis and antimycobacterial activity of 1-(β-d-Ribofuranosyl)-4-coumarinyloxymethyl-/ -coumarinyl-1,2,3-triazole, Eur J Med Chem, 150 (2018) 268-281.
[44] Y. Hu, Y. Shen, X. Wu, X. Tu, G.X. Wang, Synthesis and biological evaluation of coumarin derivatives containing imidazole skeleton as potential antibacterial agents, Eur J Med Chem, 143 (2018) 958-969.
[45] B. Inturi, G.V. Pujar, M.N. Purohit, V.B. Iyer, S. G. S, M. Kulkarni, Design, synthesis and evaluation of diphenyl ether analogues as antitubercular agents, RSC Advances, 6 (2016) 110571-110582.

[46] S.L. Kostiuk, T. Woodcock, L.F. Dudin, P.D. Howes, D.C. Harrowven, Unified syntheses of cavicularin and riccardin C: addressing the synthesis of an arene adopting a boat configuration, Chemistry, 17 (2011) 10906-10915.
[47] J. Arcau, V. Andermark, E. Aguiló, A. Gandioso, A. Moro, M. Cetina, J.C. Lima, K. Rissanen, I. Ott, L. Rodríguez, Luminescent alkynyl-gold(i) coumarin derivatives and their biological activity, Dalton Transactions, 43 (2014) 4426-4436.
[48] M. Ferraroni, F. Carta, A. Scozzafava, C.T. Supuran, Thioxocoumarins Show an Alternative Carbonic Anhydrase Inhibition Mechanism Compared to Coumarins, Journal of Medicinal Chemistry, 59 (2016) 462-473.
[49] Y. Zhao, H.S. Kim, X. Zou, L. Huang, X. Liang, Z. Li, J.S. Kim, W. Lin, Harnessing Dual-Fluorescence Lifetime Probes to Validate Regulatory Mechanisms of Organelle Interactions, Journal of the American Chemical Society, 144 (2022) 20854-20865.
[50] C.W. Tornøe, C. Christensen, M. Meldal, Peptidotriazoles on solid phase: [1,2,3]-triazoles by regiospecific copper(i)-catalyzed 1,3-dipolar cycloadditions of terminal alkynes to azides, J Org Chem, 67 (2002) 3057-3064.
[51] V.V. Rostovtsev, L.G. Green, V.V. Fokin, K.B. Sharpless, A stepwise huisgen cycloaddition process: copper(I)-catalyzed regioselective "ligation" of azides and terminal alkynes, Angew Chem Int Ed Engl, 41 (2002) 2596-2599.
[52] L. Zhang, X. Chen, P. Xue, H.H.Y. Sun, I.D. Williams, K.B. Sharpless, V.V. Fokin, G. Jia, Ruthenium-Catalyzed Cycloaddition of Alkynes and Organic Azides, Journal of the American Chemical Society, 127 (2005) 15998-15999.
[53] K. Tahlan, R. Wilson, D.B. Kastrinsky, K. Arora, V. Nair, E. Fischer, S.W. Barnes, J.R. Walker, D. Alland, C.E. Barry, 3rd, H.I. Boshoff, SQ109 targets MmpL3, a membrane transporter of trehalose monomycolate involved in mycolic acid donation to the cell wall core of Mycobacterium tuberculosis, Antimicrobial agents and chemotherapy, 56 (2012) 1797-1809.
[54] A.E. Grzegorzewicz, H. Pham, V.A. Gundi, M.S. Scherman, E.J. North, T. Hess, V. Jones, V. Gruppo, S.E. Born, J. Korduláková, S.S. Chavadi, C. Morisseau, A.J. Lenaerts, R.E. Lee, M.R. McNeil, M. Jackson, Inhibition of mycolic acid transport across the Mycobacterium tuberculosis plasma membrane, Nature chemical biology, 8 (2012) 334-341.
[55] W. Li, A. Obregón-Henao, J.B. Wallach, E.J. North, R.E. Lee, M. Gonzalez-Juarrero, D. Schnappinger, M. Jackson, Therapeutic Potential of the Mycobacterium tuberculosis Mycolic Acid Transporter, MmpL3, Antimicrobial agents and chemotherapy, 60 (2016) 5198-5207.
[56] A.D. Martin, R.A. Boulos, K.A. Stubbs, C.L. Raston, Phosphonated calix[4]arene-based amphiphiles as scaffolds for fluorescent nano-fibres, Chemical Communications, 47 (2011) 7329-7331.
[57] A. Makriyannis, S.P. Nikas, C.T. Iliopoulos, S. Kulkarni, L. Ji, Novel labelled cannabinergic ligands and related analogs, US20210300937, 2021
[58] T. Legigan, E. Migianu-Griffoni, M.A. Redouane, A. Descamps, J. Deschamp, O. Gager, M. Monteil, F. Barbault, M. Lecouvey, Synthesis and preliminary anticancer evaluation of new triazole bisphosphonate-based isoprenoid biosynthesis inhibitors, Eur J Med Chem, 214 (2021) 113241.
[59] E.F. Pettersen, T.D. Goddard, C.C. Huang, G.S. Couch, D.M. Greenblatt, E.C. Meng, T.E. Ferrin, UCSF Chimera--a visualization system for exploratory research and analysis, Journal of computational chemistry, 25 (2004) 1605-1612.
[60] E.C. Meng, E.F. Pettersen, G.S. Couch, C.C. Huang, T.E. Ferrin, Tools for integrated sequence-structure analysis with UCSF Chimera, BMC Bioinformatics, 7 (2006) 339.
[61] R. Thomsen, M.H. Christensen, MolDock: a new technique for high-accuracy molecular docking, J Med Chem, 49 (2006) 3315-3321.
[62] H. Doğan, Ş.D. Doğan, M.G. Gündüz, V.S. Krishna, C. Lherbet, D. Sriram, O. Şahin, E. Sarıpınar, Discovery of hydrazone containing thiadiazoles as Mycobacterium tuberculosis growth and enoyl acyl carrier protein reductase (InhA) inhibitors, European Journal of Medicinal Chemistry, 188 (2020).
[63] C. Vonrhein, C. Flensburg, P. Keller, A. Sharff, O. Smart, W. Paciorek, T. Womack, G. Bricogne, Data processing and analysis with the autoPROC toolbox, Acta crystallographica. Section D, Biological crystallography, 67 (2011) 293-302.

[64] I.J. Tickle, C. Flensburg, P. Keller, W. Paciorek, A. Sharff, C. Vonrhein, G. Bricogne, STARANISO. Cambridge, United Kingdom: Global Phasing Ltd, in, 2018.
[65] W. Kabsch, XDS, Acta crystallographica. Section D, Biological crystallography, 66 (2010) 125-132.
[66] A. Vagin, A. Teplyakov, Molecular replacement with MOLREP, Acta crystallographica. Section D, Biological crystallography, 66 (2010) 22-25.
[67] G. Bricogne, E. Blanc, M. Brandl, C. Flensburg, P. Keller, W. Paciorek, P. Roversi, A. Sharff, O.S. Smart, C. Vonrhein, T.O. Womack, BUSTER version 2.10.4. Cambridge, United Kingdom: Global Phasing Ltd, in, 2017

[68] O.S. Smart, A. Sharff, J. Holstein, T.O. Womack, C. Flensburg, P. Keller, W. Paciorek, C. Vonrhein, G. Bricogne, Grade2 version 1.3, in, 2021.
[69] P. Emsley, K. Cowtan, Coot: model-building tools for molecular graphics, Acta crystallographica. Section D, Biological crystallography, 60 (2004) 2126-2132.
[70] N.H. Le, P. Constant, S. Tranier, V. Nahoum, V. Guillet, L. Maveyraud, M. Daffé, L. Mourey, P. Verhaeghe, H. Marrakchi, Drug screening approach against mycobacterial fatty acyl-AMP ligase FAAL32 renews the interest of the salicylanilide pharmacophore in the fight against tuberculosis, Bioorg Med Chem, 71 (2022) 116938.
[71] B. Phetsuksiri, A.R. Baulard, A.M. Cooper, D.E. Minnikin, J.D. Douglas, G.S. Besra, P.J. Brennan, Antimycobacterial activities of isoxyl and new derivatives through the inhibition of mycolic acid synthesis, Antimicrobial agents and chemotherapy, 43 (1999) 1042-1051.
[72] V. Pflégr, L. Horváth, J. Stolaříková, A. Pál, J. Korduláková, S. Bősze, J. Vinšová, M. Krátký, Design and synthesis of 2-(2-isonicotinoylhydrazineylidene)propanamides as InhA inhibitors with high antitubercular activity, Eur J Med Chem, 223 (2021) 113668.
[73] A.E. Grzegorzewicz, J. Korduláková, V. Jones, S.E. Born, J.M. Belardinelli, A. Vaquié, V.A. Gundi, J. Madacki, N. Slama, F. Laval, J. Vaubourgeix, R.M. Crew, B. Gicquel, M. Daffé, H.R. Morbidoni, P.J. Brennan, A. Quémard, M.R. McNeil, M. Jackson, A common mechanism of inhibition of the Mycobacterium tuberculosis mycolic acid biosynthetic pathway by isoxyl and thiacetazone, J Biol Chem, 287 (2012) 38434-38441.
[74] M.H. Larsen, C. Vilchèze, L. Kremer, G.S. Besra, L. Parsons, M. Salfinger, L. Heifets, M.H. Hazbon, D. Alland, J.C. Sacchettini, W.R. Jacobs, Jr., Overexpression of inhA, but not kasA, confers resistance to isoniazid and ethionamide in Mycobacterium smegmatis, M. bovis BCG and M. tuberculosis, Mol Microbiol, 46 (2002) 453-466.
[75] V. Vichai, K. Kirtikara, Sulforhodamine B colorimetric assay for cytotoxicity screening, Nature protocols, 1 (2006) 1112-1116.